

## A Triangular Plate Element with Drilling Degrees of Freedom, for Large Rotation Analyses of Built-up Plate/Shell Structures, Based on the Reissner Variational Principle and the von Karman Nonlinear Theory in the Co-rotational Reference Frame

Y.C. Cai<sup>1,2</sup>, J.K. Paik<sup>3</sup> and S.N. Atluri<sup>2</sup>

**Abstract:** This paper presents an elementary finite element method for geometrically nonlinear large rotation analyses of built-up plate/shell structures comprising of thin members. The tangent stiffness matrix of the element in the updated Lagrangian co-rotational reference frame is developed, based on the von Karman nonlinear theory of plates, and the Reissner variational principle, allowing for unsymmetric stresses and drilling rotations, useful in the analysis of built-up plate and shell structure. The finite rotation of the co-rotational reference frame relative to a globally fixed Cartesian frame, is simply determined from the finite displacement vectors of the nodes of the element in the global reference frame, thus allowing for an elementary transformation of the tangent stiffness matrix from the updated co-rotational reference frame to the globally fixed Cartesian frame. The element employed here is a 3-node plate element with 6 degrees of freedom per node, including 1 drilling degree of freedom and 5 degrees of freedom [3 displacements, and the derivatives of the transverse displacement around two independent axes in the plane of the plate in the co-rotational reference frame]. The  $(18 \times 18)$  tangent stiffness matrices of the plate element in the updated Lagrangian co-rotational reference frame are derived, based on the assumptions that: (1) the inplane stress resultants  $N_{\alpha\beta}$  (unsymmetric) are constant in each element; (2) the bending moments  $M_{\alpha\beta}$  (symmetric) are linear and  $C^0$  within each element; and (3) the transverse rotations  $\theta_i$  (including the drilling degrees of  $\theta_3$ ) are linear and  $C^0$  within each element. When compared to the primal approach wherein  $C^1$  continuous trial functions for transverse displacements over each element are necessary, the trial functions for

---

<sup>1</sup> Key Laboratory of Geotechnical and Underground Engineering of Ministry of Education, Department of Geotechnical Engineering, Tongji University, Shanghai 200092, P.R.China

<sup>2</sup> Center for Aerospace Research & Education, University of California, Irvine

<sup>3</sup> Lloyd's Register Educational Trust (LRET) Center of Excellence, Pusan National University, Korea

the transverse bending moments and the rotations are very simple in the current approach, and can be assumed to be linear within each element. The present ( $18 \times 18$ ) tangent stiffness matrices of the plate, based on the Reissner variational principle and the von Karman type simplified nonlinear plate theory in the co-rotational reference frame, lead to analyses, which are much simpler and more physically-based, than many others in the literature for large rotation/deformation analysis of built-up plate/shell structures [such as component plates joined at an angle]. Numerical examples demonstrate the accuracy and robustness of the present method.

**Keywords:** large deformation, thin plate/shell, explicit tangent stiffness, updated Lagrangian formulation, Reissner variational principle, drilling degrees of freedom.

## 1 Introduction

Most of the developments on computational (mostly finite element) analysis of large deformations (rotations) of plates and shells in the period 1980-2010 have concentrated on highly mathematical discourses on differential geometry and group-theoretical considerations of finite rotations, etc [see for instance Atluri (1984), Atluri and Cazzani (1994), Simo(1993), Iura and Atluri (Special Issue of CMES, 2003)]. Among the non-standard (i.e., other than those based on the classical potential energy method) finite element approaches, Punch and Atluri (1984) examined the performance of linear and quadratic Serendipity hybrid-stress 2D and 3D beam elements. Kondoh, Tanaka and Atluri (1986), Kondoh and Atluri (1987), Shi and Atluri(1988), Iura and Atluri (1988), Crisfield (1990) presented the derivations of explicit expressions of the tangent stiffness matrices for beams undergoing large displacements, without employing either numerical or symbolic integration. A number of plate/shell elements have also been developed for the analyses of plate/shell structures [see a survey by Yang, Saigal, Masud, and Kapania (2000)]. Shi and Voyiadzis (1991), Huang, Shenoy and Atluri (1994), and Pian (1964) proposed some hybrid plate element based on assumed strain distributions or hybrid principles. A few studies, such as Allman (1988), Iura and Atluri (1992), Nguyen-Van, Mai-Duy and Tran-Cong (2009) employed the drilling degrees of freedom in plate/shell elements, using the potential energy principle to avoid the problem of singularity in the stiffness matrix. Atluri and his co-workers (Atluri 1980; Atluri 1984; Atluri and Cazzani 1994) extensively studied the large rotations in plates and shells, and attendant mixed variational principles involving the rotation tensor as a direct variable along with the stress-resultant tensor and the stress-couple tensor. These diverse theories and methods of the plate/shell have now been widely applied to a variety of problems.

Although a large number of different efforts have been made, some inherent difficulties related to the linear/nonlinear analyses of 3D frame/plate/shell structures still need to be further overcome. The objective of the present paper is to provide an *essentially elementary engineering treatment of plates and shells undergoing large deformations and rotations* without resorting to the highly mathematical tools of differential geometry, and group –theoretical treatment of finite rotations, as in most of the prior literature. This paper presents an elementary finite element method for large deformation /large rotation analyses of built-up plate/shell structures comprising of thin members. The tangent stiffness matrix of the element in the updated Lagrangian co-rotational referenced frame is developed based on the von Karman nonlinear theory of plates, and the Reissner variational principle, allowing for unsymmetric stresses and drilling rotations, to facilitate the analysis of built-up plate and shell structures. The finite rotation of the co-rotational reference frame relative to a globally fixed Cartesian frame, is simply determined from the finite displacement vectors of the nodes of the element in the global reference frame, thus allowing for a simple transformation of the tangent stiffness matrix from the updated co-rotational reference frame to the globally fixed Cartesian frame. The element employed here is a 3-node plate element with 6 degrees of freedom per node, including 1 drilling degree of freedom and 5 degrees of freedom [3 displacements, and the derivatives of the transverse displacement around two independent axes in the plane of the element in the updated Lagrangian reference frame]. The  $(18 \times 18)$  tangent stiffness matrices of the plate element in the updated Lagrangian reference frame are derived, based on the assumptions that: (1) the inplane stress resultants  $N_{\alpha\beta}$  (unsymmetric) are constant in each element; (2) the bending moments  $M_{\alpha\beta}$  (symmetric) are linear and  $C^0$  within each element; and (3) the transverse rotations  $\theta_i$  (including the drilling degrees of  $\theta_3$ ) are linear and  $C^0$  within each element. When compared to the primal approach wherein  $C^1$  continuous trial functions for transverse displacements over each element are necessary, the trial functions for the transverse bending moments and the rotations are very simple in the current approach, and can be assumed to be linear within each element. The present  $(18 \times 18)$  tangent stiffness matrices of the plate are much simpler than those of many others in the literature for large rotation/deformation analysis of plate/shell structures. Numerical examples demonstrate the accuracy and robust of the present method.

In summary, the present method for large deformation /large rotation analysis of built-up plate and shell structures is based on the incorporation of all the following simple features, each of which has an elementary engineering basis:

1. The use of the mathematical theories of differential geometry, and group theoretical methods to characterize finite rotations is eliminated;

2. The tangent stiffness matrix of a 3 noded, 18 d.o.f. plate element, in the updated Lagrangian reference frame, is developed based on the von Karman nonlinear plate theory.
3. Drilling degrees of freedom at each of the 3-nodes of the plate element are part of the 18 d.o.f. of the element. This facilitates the analysis of built-up plate and shell structures.
4. The tangent stiffness matrix of the plate element in the updated Lagrangian reference frame is derived based on the Reissner variational principle. In this variational principle,  $N_{\alpha\beta}$  (which are unsymmetric) are assumed to be constant within each 3-noded element;  $M_{\alpha\beta}$  (which are symmetric) are assumed to be linear within each element; the drilling rotation, as well as the derivatives of the transverse displacement in each in-plane direction of the plate in the updated Lagrangian co-rotational reference frame are assumed to be linear in each element.
5. In the present mixed formulation, the transverse displacement in the interior of the element does not appear and need not to be assumed. This is in contrast to the potential energy principle wherein a  $C^1$  continuous transverse displacement needs to be assumed over the element.
6. The finite rotation of the base-vectors in the plane of the plate-element and that normal to it, in the updated Lagrangian co-rotational frame, from the base vectors of the global Cartesian reference frame, is simply determined from the finite displacement vectors of the nodes of the element, in a very elementary way. Thus, complicated descriptions of finite rotation vectors and group theoretical methods, are simply avoided.
7. The transformation of the  $(18 \times 18)$  tangent stiffness matrix of the plate element from the reference axes in the updated Lagrangian reference frame to the global Cartesian reference frame is accomplished in a very elementary way.

Thus, each of the above steps is quite elementary, but their simultaneous employment leads to a simplified analysis of large rotations and large displacements of built-up plate and shell structures. While one or a few of the above steps may have been explored in prior literature, by others as well as the authors, a combination of all the above steps is new, and is the contribution of the present work. While the present work is limited to elastic materials undergoing large deformations, the extension to inelasticity is straight forward and will be pursued in forthcoming publications.

**2 Von-Karman nonlinear theory for a plate undergoing moderately large deformations in the updated Lagrangian co-rotational reference frame**

We consider a fixed global reference frame with axes  $\bar{x}_i (i = 1, 2, 3)$  and base vectors  $\bar{\mathbf{e}}_i$ . The plate in its undeformed state, with local coordinates  $\tilde{x}_i (i = 1, 2, 3)$  and base vectors  $\tilde{\mathbf{e}}_i$ , is located arbitrarily in space, as shown in Fig.1. The current configuration of the plate, after arbitrarily large deformations, is also shown in Fig.1. The local coordinates in the reference frame in the current configuration are  $x_i$  and the base vectors are  $\mathbf{e}_i (i = 1, 2, 3)$ .

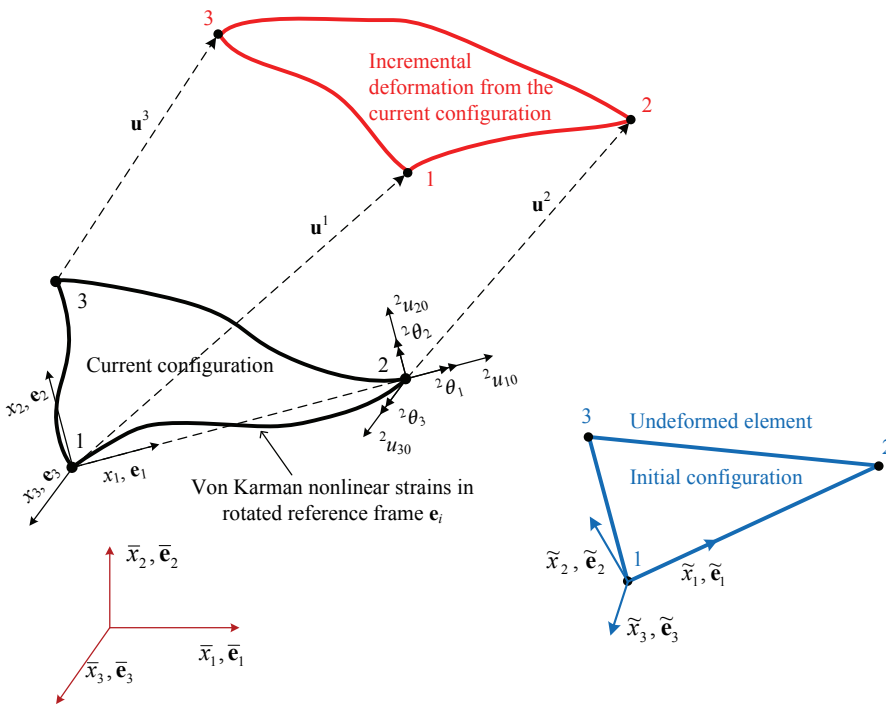


Figure 1: Updated Lagrangian co-rotational reference frame for a plate element

As shown in Fig.2, we consider the large deformations of a typical thin plate. A von-Karman type deformation is assumed for the continued deformation from the current configuration, in the co-rotational frame of reference  $\mathbf{e}_i (i = 1, 2, 3)$  in the local coordinates  $x_i (i = 1, 2, 3)$ . If  $h$  is the characteristic thick of thin plate, and  $u_i(x_j)$  are the displacements of the plate from the current configuration in the  $\mathbf{e}_i$  directions, the precise assumptions governing the continued deformations from the current configuration are  $(\alpha = 1, 2; \beta = 1, 2, 3)$

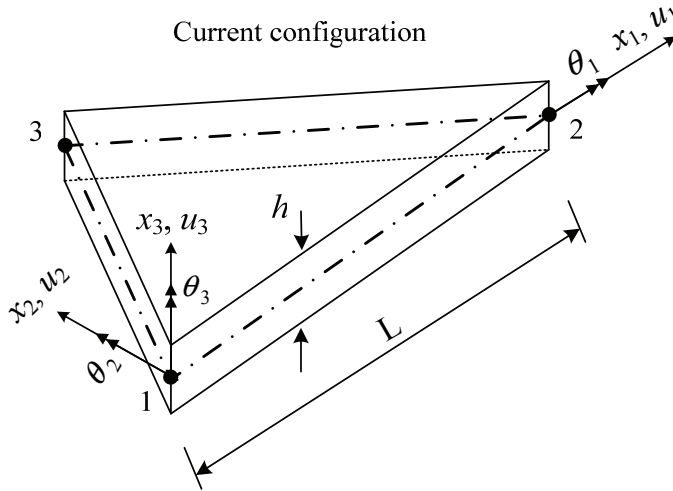


Figure 2: Large deformation analysis model of a plate element

1.  $\frac{h}{L} \leq 1$  (the plate is thin);
2.  $u_3/h \sim O(1)$ ;
3.  $\left(\frac{\partial u_3}{\partial x_\alpha}\right) \ll 1$ ;
4.  $u_\alpha/h \ll 1$ ;
5.  $\frac{\partial u_\alpha}{\partial x_\beta}$  are much smaller than  $\frac{\partial u_3}{\partial x_\alpha}$ ;  $\left(\frac{\partial u_\alpha}{\partial x_\beta}\right)^2 \leq \left(\frac{\partial u_3}{\partial x_\alpha}\right)^2$  only  $\left(\frac{\partial u_3}{\partial x_\alpha}\right)^2$  are retained as nonlinear terms in the co-rotational frame of reference;
6. All strains  $E_{\alpha\beta} \leq 1$  [where  $E_{\alpha\beta}$  are strains from the current configuration, in the  $x_\alpha$  coordinates];
7. The material is linear. For an elastic-plastic material, the rate relation is bi-linear.

Thus, the generally 3-dimensional displacement state in the  $e_i$  system is simplified to be of the type

$$\begin{aligned} u_1 &= u_{10}(x_\alpha) - x_3 \frac{\partial u_3}{\partial x_1} \\ u_2 &= u_{20}(x_\alpha) - x_3 \frac{\partial u_3}{\partial x_2} \end{aligned} \quad (1)$$

where

$$\begin{aligned} u_3 &= u_{30}(x_1, x_2) \\ u_{10} &= u_{10}(x_1, x_2) \\ u_{20} &= u_{20}(x_1, x_2) \end{aligned} \tag{2}$$

**2.1 Strain-displacement relations**

Considering only von Karman type nonlinearities in the rotated reference frame  $\mathbf{e}_i(x_i)$ , we can write the Green-Lagrange strain-displacement relations in the updated Lagrangian co-rotational frame  $\mathbf{e}_i$  in Fig.1 as:

$$\begin{aligned} E_{11} &= \frac{\partial u_1}{\partial x_1} + \frac{1}{2} \left( \frac{\partial u_1}{\partial x_1} \right)^2 + \frac{1}{2} \left( \frac{\partial u_2}{\partial x_1} \right)^2 + \frac{1}{2} \left( \frac{\partial u_3}{\partial x_1} \right)^2 \\ &\cong \frac{\partial u_{10}}{\partial x_1} - x_3 \frac{\partial^2 u_{30}}{\partial x_1^2} + \frac{1}{2} \left( \frac{\partial u_{30}}{\partial x_1} \right)^2 \\ E_{22} &= \frac{\partial u_2}{\partial x_2} + \frac{1}{2} \left( \frac{\partial u_1}{\partial x_2} \right)^2 + \frac{1}{2} \left( \frac{\partial u_2}{\partial x_2} \right)^2 + \frac{1}{2} \left( \frac{\partial u_3}{\partial x_2} \right)^2 \\ &\cong \frac{\partial u_{20}}{\partial x_2} - x_3 \frac{\partial^2 u_{30}}{\partial x_2^2} + \frac{1}{2} \left( \frac{\partial u_{30}}{\partial x_2} \right)^2 \\ E_{12} &= \frac{\partial u_1}{\partial x_2} + \theta_3 + \frac{1}{2} \left[ \frac{\partial u_1}{\partial x_1} \frac{\partial u_1}{\partial x_2} + \frac{\partial u_2}{\partial x_1} \frac{\partial u_2}{\partial x_2} + \frac{\partial u_3}{\partial x_1} \frac{\partial u_3}{\partial x_2} \right] \\ &\cong \frac{\partial u_{10}}{\partial x_2} - x_3 \frac{\partial^2 u_{30}}{\partial x_1 \partial x_2} + \theta_3 + \frac{1}{2} \frac{\partial u_{30}}{\partial x_1} \frac{\partial u_{30}}{\partial x_2} \\ E_{21} &= \frac{\partial u_2}{\partial x_1} - \theta_3 + \frac{1}{2} \left[ \frac{\partial u_1}{\partial x_1} \frac{\partial u_1}{\partial x_2} + \frac{\partial u_2}{\partial x_1} \frac{\partial u_2}{\partial x_2} + \frac{\partial u_3}{\partial x_1} \frac{\partial u_3}{\partial x_2} \right] \\ &\cong \frac{\partial u_{20}}{\partial x_1} - x_3 \frac{\partial^2 u_{30}}{\partial x_1 \partial x_2} - \theta_3 + \frac{1}{2} \frac{\partial u_{30}}{\partial x_1} \frac{\partial u_{30}}{\partial x_2} \neq E_{12} \\ E_{33} &= \frac{\partial u_3}{\partial x_3} + \frac{1}{2} \left( \frac{\partial u_1}{\partial x_3} \right)^2 + \frac{1}{2} \left( \frac{\partial u_2}{\partial x_3} \right)^2 + \frac{1}{2} \left( \frac{\partial u_3}{\partial x_3} \right)^2 \approx 0 \\ E_{13} &= \frac{1}{2} \left[ \frac{\partial u_1}{\partial x_3} + \frac{\partial u_3}{\partial x_1} + \frac{\partial u_1}{\partial x_1} \frac{\partial u_1}{\partial x_3} + \frac{\partial u_2}{\partial x_1} \frac{\partial u_2}{\partial x_3} + \frac{\partial u_3}{\partial x_1} \frac{\partial u_3}{\partial x_3} \right] \approx 0 \\ E_{23} &= \frac{1}{2} \left[ \frac{\partial u_2}{\partial x_3} + \frac{\partial u_3}{\partial x_2} + \frac{\partial u_1}{\partial x_2} \frac{\partial u_1}{\partial x_3} + \frac{\partial u_2}{\partial x_2} \frac{\partial u_2}{\partial x_3} + \frac{\partial u_3}{\partial x_2} \frac{\partial u_3}{\partial x_3} \right] \approx 0 \end{aligned} \tag{3}$$

where  $\theta_3 = \frac{1}{2} \left( \frac{\partial u_2}{\partial x_1} - \frac{\partial u_1}{\partial x_2} \right)$  is the drilling degree of freedom.

Eq.(3) is also called the Kirchhoff hypothesis of deformation for thin plates, where

“normals remain normal”, and the strain-displacement relations are attributed to von Karman.

### 2.2 Stress-Strain relations

The stress-measure conjugate to these strains is the second Piola-Kirchhoff stress tensor  $\mathbf{S}^1 [S_{ij}^1]$ .

For an isotropic linear elastic material,

$$S_{11}^1 = 2\mu E_{11} + \lambda (E_{11} + E_{22}) = (2\mu + \lambda) E_{11} + \lambda E_{22} \tag{4}$$

where

$$\begin{aligned} \mu &= \frac{E}{2(1+\nu)} \\ \lambda &= \frac{E\nu}{(1+\nu)(1-2\nu)} \end{aligned} \tag{5}$$

$E$  is the elastic modulus;  $\nu$  is the Poisson ratio.

We also note that

$$S_{33}^1 = 2\mu E_{33} + \lambda (E_{11} + E_{22})$$

can be large.

Nevertheless, use of 3-D constitutive law for plate is not desirable. We want  $S_{33}^1 \cong 0$ ,  $S_{13}^1 \cong 0$  and  $S_{23}^1 \cong 0$ . [Note, however, that while the transverse shear-stresses  $S_{13}^1$  and  $S_{23}^1$  are assumed to be zero, their integrals in thickness direction, namely  $Q_{13}^1$  and  $Q_{23}^1$  the transverse shear forces in the  $x_3$  direction, cannot be zero. Otherwise, the plate cannot be in equilibrium. This is an inherent inconsistency in the plate theory.]

Thus, while the geometric theory of strain in the Kirchhoff plate leads to:

$$E_{\alpha\beta} \neq 0 \quad E_{3i} = 0$$

implying a state of “plane strain”, a mechanical theory of stress leads to the assumption that:

$$S_{\alpha\beta}^1 \neq 0 \quad S_{3i}^1 \cong 0$$

implying a state of “plane stress”. This is an inherent/unavoidable inconsistency in the engineering theory of plates.

We assume a state of plane-stress to derive the stresses from strains in a thin plate as

$$\begin{aligned}
 S_{11}^1 &= \frac{E}{1-\nu^2} [E_{11} + \nu E_{22}] \\
 S_{22}^1 &= \frac{E}{1-\nu^2} [E_{22} + \nu E_{11}] \\
 S_{12}^1 &= \frac{E}{1+\nu} E_{12} \\
 S_{21}^1 &= \frac{E}{1+\nu} E_{21} \neq S_{12}^1 \\
 S_{33}^1 &= S_{13}^1 = S_{23}^1 = 0 \text{ (They can be determined from} \\
 &\quad \text{equilibrium equations)}
 \end{aligned} \tag{6}$$

If the mid-surface of the plate is taken as the reference plane in the co-rotational updated Lagrangian reference frame, the generalized forces of the plate in Fig.2 can be defined as

$$\begin{aligned}
 N_{11} &= C \left[ u_{10,1} + \nu u_{20,2} + \frac{1}{2} (u_{30,1})^2 + \frac{\nu}{2} (u_{30,2})^2 \right] \\
 N_{22} &= C \left[ u_{20,2} + \nu u_{10,1} + \frac{1}{2} (u_{30,2})^2 + \frac{\nu}{2} (u_{30,1})^2 \right] \\
 N_{12} &= (1-\nu) C \left[ u_{10,2} + \theta_3 + \frac{1}{2} u_{30,1} u_{30,2} \right] \\
 N_{21} &= (1-\nu) C \left[ u_{20,1} - \theta_3 + \frac{1}{2} u_{30,1} u_{30,2} \right] \\
 M_{11} &= -D [u_{30,11} + \nu u_{30,22}] \\
 M_{22} &= -D [u_{30,22} + \nu u_{30,11}] \\
 M_{12} &= M_{21} = -(1-\nu) D u_{30,12}
 \end{aligned} \tag{7}$$

where  $,i$  denotes a differentiation with respect to  $x_i$ ,  $C = \frac{Eh}{1-\nu^2}$ , and  $D = \frac{Eh^3}{12(1-\nu^2)}$ .

The matrix form of the above equations is

$$\boldsymbol{\sigma} = \mathbf{D}\boldsymbol{\varepsilon} \tag{8}$$

where  $\boldsymbol{\sigma}$  are the element generalized stresses,  $\boldsymbol{\varepsilon}$  are the element generalized strains,

and

$$\boldsymbol{\sigma} = \begin{pmatrix} \sigma_1 \\ \sigma_2 \\ \sigma_3 \\ \sigma_4 \\ \sigma_5 \\ \sigma_6 \\ \sigma_7 \end{pmatrix} = \begin{pmatrix} N_{11} \\ N_{22} \\ N_{12} \\ N_{21} \\ M_{11} \\ M_{22} \\ M_{12} \end{pmatrix} \tag{9}$$

$$\boldsymbol{\varepsilon} = \begin{pmatrix} \varepsilon_1 \\ \varepsilon_2 \\ \varepsilon_3 \\ \varepsilon_4 \\ \varepsilon_5 \\ \varepsilon_6 \\ \varepsilon_7 \end{pmatrix} = \boldsymbol{\varepsilon}^L + \boldsymbol{\varepsilon}^N = \begin{pmatrix} u_{10,1} \\ u_{20,2} \\ u_{10,2} + \theta_3 \\ u_{20,1} - \theta_3 \\ -u_{30,11} \\ -u_{30,22} \\ -2u_{30,12} \end{pmatrix} + \begin{pmatrix} (u_{30,1})^2/2 \\ (u_{30,2})^2/2 \\ u_{30,1}u_{30,2}/2 \\ u_{30,1}u_{30,2}/2 \\ 0 \\ 0 \\ 0 \end{pmatrix} \tag{10}$$

$$\mathbf{D} = \begin{bmatrix} C & \nu C & 0 & 0 & 0 & 0 & 0 \\ \nu C & C & 0 & 0 & 0 & 0 & 0 \\ 0 & 0 & C_1 & 0 & 0 & 0 & 0 \\ 0 & 0 & 0 & C_1 & 0 & 0 & 0 \\ 0 & 0 & 0 & 0 & D & \nu D & 0 \\ 0 & 0 & 0 & 0 & \nu D & D & 0 \\ 0 & 0 & 0 & 0 & 0 & 0 & D_1 \end{bmatrix} \tag{11}$$

where  $C_1 = (1 - \nu)C$  and  $D_1 = (1 - \nu)D/2$ .

### 3 Updated Lagrangian formulation in the co-rotational reference frame $\mathbf{e}_i$ , to determine the tangent stiffness matrix in the $\mathbf{e}_i$ frame

#### 3.1 The use of the Reissner variational principle in the co-rotational updated Lagrangian reference frame

If  $\tau_{ij}^0$  are the initial Cauchy stresses in the co-rotational updated Lagrangian reference coordinates  $\mathbf{e}_i$  of Fig.1,  $S_{ij}^1$  are the additional (incremental) second Piola-Kirchhoff stresses in the same co-rotational updated Lagrangian reference frame with axes  $\mathbf{e}_i$ ,  $S_{ij} = S_{ij}^1 + \tau_{ij}^0$  are the total stresses, and  $u_i$  are the incremental displacements in the co-rotational updated-Lagrangian reference frame, the functional of the Reissner variational principle (Reissner 1953) [see also Atluri and Reissner

(1989)] for the incremental  $S_{ij}^1$  and  $u_i$  in the co-rotational updated Lagrangian reference frame is given by [Atluri 1979, 1980]

$$\begin{aligned} \Pi_R = \int_V \left\{ -B(S_{11}^1, S_{12}^1, S_{21}^1, S_{22}^1) + \frac{1}{2} \tau_{ij}^0 u_{k,i} u_{k,j} + [S_{11} u_{1,1} + S_{22} u_{2,2} \right. \\ \left. + S_{12} (u_{1,2} + \theta_3) + S_{21} (u_{2,1} - \theta_3)] - \rho b_i u_i \right\} dV - \int_{S_\sigma} \bar{T}_i u_i dS \end{aligned} \quad (12)$$

Where  $V$  is the volume in the current co-rotational reference state,  $S_\sigma$  is the surface where tractions are prescribed,  $b_i = b_i^0 + b_i^1$  are the body forces per unit volume in the current reference state, and  $\bar{T}_i = \bar{T}_i^0 + \bar{T}_i^1$  are the given boundary tractions.

The conditions of stationarity of  $\Pi_R$ , with respect to variations  $\delta S_{ij}^1$  and  $\delta u_i$  lead to the following incremental equations in the co-rotational updated- Lagrangian reference frame.

$$\frac{\partial B}{\partial S_{11}^1} = u_{1,1}; \quad \frac{\partial B}{\partial S_{22}^1} = u_{2,2}; \quad \frac{\partial B}{\partial S_{12}^1} = u_{1,2} + \theta_3; \quad \frac{\partial B}{\partial S_{21}^1} = u_{2,1} - \theta_3 \quad (13)$$

$$\left[ S_{kj}^1 + \frac{1}{2} (\tau_{ij}^0 + \tau_{ji}^0) u_{k,i} \right]_{,j} + \rho b_k^1 = - (\tau_{kj}^0)_{,j} - \rho b_k^0; \quad S_{12} = S_{21} \quad (14)$$

$$n_j \left[ S_{kj}^1 + \frac{1}{2} (\tau_{ij}^0 + \tau_{ji}^0) u_{k,i} \right] - \bar{T}_k^1 = -n_j \tau_{kj}^0 + \bar{T}_k^0 \text{ at } S_\sigma \quad (15)$$

In Eq.(12), the displacement boundary conditions,

$$u_i = \bar{u}_i \text{ at } S_u \quad (16)$$

are assumed to be satisfied a priori, at the external boundary,  $S_u$ . Eq.(14) leads to equilibrium correction iterations.

If the variational principle embodied in Eq.(12) is applied to a group of finite elements,  $V_m, m = 1, 2, \dots, N$ , which comprise the volume  $V$ , ie,  $V = \sum V_m$ , then

$$\begin{aligned} \Pi_R = \sum_m \left( \int_{V_m} \left\{ -B(S_{11}^1, S_{12}^1, S_{21}^1, S_{22}^1) + \frac{1}{2} \tau_{ij}^0 u_{k,i} u_{k,j} + [S_{11} u_{1,1} + S_{22} u_{2,2} \right. \right. \\ \left. \left. + S_{12} (u_{1,2} + \theta_3) + S_{21} (u_{2,1} - \theta_3)] - \rho b_i u_i \right\} dV - \int_{S_\sigma} \bar{T}_i u_i dS \right) \end{aligned} \quad (17)$$

Let  $\partial V_m$  be the boundary of  $V_m$ , and  $\rho_m$  be the part of  $\partial V_m$  which is shared by the element with its neighbouring elements. If the trial function  $u_i$  and the test function  $\partial u_i$  in each  $V_m$  are such that the inter-element continuity condition,

$$u_i^+ = u_i^- \text{ at } \rho_m \tag{18}$$

(where + and – refer to either side of the boundary  $\rho_m$ ) is satisfied a priori, then it can be shown (Atluri 1975,1984; Atluri and Murakawa 1977; Atluri, Gallagher and Zienkiewicz 1983) that the conditions of stationarity of  $\Pi_R$  in Eq.(17) lead to:

$$\frac{\partial B}{\partial S_{11}^1} = u_{1,1}; \frac{\partial B}{\partial S_{22}^1} = u_{2,2}; \frac{\partial B}{\partial S_{12}^1} = u_{1,2} + \theta_3; \frac{\partial B}{\partial S_{21}^1} = u_{2,1} - \theta_3 \text{ in } V_m \tag{19}$$

$$\left[ S_{kj}^1 + \frac{1}{2} (\tau_{ij}^0 + \tau_{ji}^0) u_{k,i} \right]_{,j} + \rho b_k^1 = - (\tau_{kj}^0)_{,j} - \rho b_k^0; S_{12} = S_{21} \text{ in } V_m \tag{20}$$

$$\left\{ n_j \left[ S_{kj}^1 + \frac{1}{2} (\tau_{ij}^0 + \tau_{ji}^0) u_{k,i} \right] \right\}^+ + \left\{ n_j \left[ S_{kj}^1 + \frac{1}{2} (\tau_{ij}^0 + \tau_{ji}^0) u_{k,i} \right] \right\}^- \text{ at } \rho_m \tag{21}$$

$$= - [n_j \tau_{kj}^0]^+ - [n_j \tau_{kj}^0]^-$$

$$n_j \left[ S_{kj}^1 + \frac{1}{2} (\tau_{ij}^0 + \tau_{ji}^0) u_{k,i} \right]^- \bar{T}_k^1 = -n_j \tau_{kj}^0 + \bar{T}_k^0 \text{ at } S_{\sigma m} \tag{22}$$

Eq.(21) is the condition of traction reciprocity at the inter-element boundary,  $\rho_m$ . Eqs.(20) and (21) lead to corrective iterations for equilibrium within each element, and traction reciprocity at the inter-element boundaries, respectively.

Carrying out the integration over the thickness of each plate element, and using Eqs.(3) and (6), Eq.(17) can be easily shown to reduce to:

$$\begin{aligned} \Pi_R &= \sum_{elem} \left\{ \int_A \left( -\frac{1}{2} \boldsymbol{\sigma}^T \mathbf{D}^{-1} \boldsymbol{\sigma} \right) dA \right. \\ &\quad + \frac{1}{2} \int_A [N_{11}^0 u_{30,1}^2 + N_{22}^0 u_{30,2}^2 + (N_{12}^0 + N_{21}^0) u_{30,1} u_{30,2}] dA \\ &\quad + \int_A (\hat{N}_{11} \boldsymbol{\varepsilon}_1^L + \hat{N}_{22} \boldsymbol{\varepsilon}_2^L + \hat{N}_{12} \boldsymbol{\varepsilon}_3^L + \hat{N}_{21} \boldsymbol{\varepsilon}_4^L + \hat{M}_{11} \boldsymbol{\varepsilon}_5 + \hat{M}_{22} \boldsymbol{\varepsilon}_6 + \hat{M}_{12} \boldsymbol{\varepsilon}_7) dA - \bar{\mathbf{Q}} \mathbf{q} \left. \right\} \\ &= \sum_{elem} (-\Pi_{R1} + \Pi_{R2} + \Pi_{R3} - \Pi_{R4}) \end{aligned} \tag{23}$$

where

$$\begin{aligned}
 \Pi_{R1} &= \frac{1}{2} \int_A (\boldsymbol{\sigma}^T \mathbf{D}^{-1} \boldsymbol{\sigma}) dA \\
 \Pi_{R2} &= \frac{1}{2} \int_A [N_{11}^0 u_{30,1}^2 + N_{22}^0 u_{30,2}^2 + (N_{12}^0 + N_{21}^0) u_{30,1} u_{30,2}] dA \\
 \Pi_{R3} &= \int_A (\hat{N}_{11} \boldsymbol{\varepsilon}_1^L + \hat{N}_{22} \boldsymbol{\varepsilon}_2^L + \hat{N}_{12} \boldsymbol{\varepsilon}_3^L + \hat{N}_{21} \boldsymbol{\varepsilon}_4^L + \hat{M}_{11} \boldsymbol{\varepsilon}_5 + \hat{M}_{22} \boldsymbol{\varepsilon}_6 + \hat{M}_{12} \boldsymbol{\varepsilon}_7) dA \\
 \Pi_{R4} &= \bar{\mathbf{Q}} \mathbf{q}
 \end{aligned} \tag{24}$$

$\mathbf{D}$  is given in Eq.(11),  $\mathbf{C} = \mathbf{D}^{-1}$ ,  $\boldsymbol{\sigma}$  is given in Eq.(9),

$$\boldsymbol{\sigma}_{ij}^0 = [N_{11}^0 \quad N_{22}^0 \quad N_{12}^0 \quad N_{21}^0 \quad M_{11}^0 \quad M_{22}^0 \quad M_{12}^0]^T$$

is the initial element-generalized- stress in the co-rotational reference coordinates  $\mathbf{e}_i$ , and  $\hat{\boldsymbol{\sigma}} = \boldsymbol{\sigma}^0 + \boldsymbol{\sigma} = [\hat{N}_{11} \quad \hat{N}_{22} \quad \hat{N}_{12} \quad \hat{N}_{21} \quad \hat{M}_{11} \quad \hat{M}_{22} \quad \hat{M}_{12}]^T$  is the total element generalized stresses in the co-rotational reference coordinates  $\mathbf{e}_i$ .  $\bar{\mathbf{Q}}$  is the nodal external generalized force vector (consisting of force as well as moments) in the global Cartesian reference frame, and  $\mathbf{q}$  is the incremental nodal generalized displacement vector (consisting of displacements as well as rotations) in the global Cartesian reference frame. It should be noted that while  $\Pi_R$  in Eq.(23) represents a sum over the elements, the relevant integrals are evaluated over each element in it's own co-rotational updated Lagrangian reference frame.

By integrating by parts, the second item of the right hand side of Eq.(23) can be written as

$$\begin{aligned}
 \int_A \hat{N}_{11} \boldsymbol{\varepsilon}_1^L dA &= \int_A \hat{N}_{11} u_{10,1} dA = - \int_A \hat{N}_{11,1} u_{10} dA + \oint_{S_e} n_1 \hat{N}_{11} u_{10} de \\
 \int_A \hat{N}_{22} \boldsymbol{\varepsilon}_2^L dA &= \int_A \hat{N}_{22} u_{20,2} dA = - \int_A \hat{N}_{22,2} u_{20} dA + \oint_{S_e} n_2 \hat{N}_{22} u_{20} de \\
 \int_A \hat{N}_{12} \boldsymbol{\varepsilon}_3^L dA &= \int_A \hat{N}_{12} (u_{10,2} + \theta_3) dA = \int_A \hat{N}_{12} \theta_3 dA - \int_A \hat{N}_{12,2} u_{10} dA + \oint_{S_e} n_2 \hat{N}_{12} u_{10} de \\
 \int_A \hat{N}_{21} \boldsymbol{\varepsilon}_4^L dA &= \int_A \vec{N}_{21} (u_{20,1} - \theta_3) dA = - \int_A \hat{N}_{21} \theta_3 dA - \int_A \hat{N}_{21,1} u_{20} dA + \oint_{S_e} n_1 \hat{N}_{21} u_{20} de
 \end{aligned}$$

$$\begin{aligned}
 & \int_A \hat{M}_{11} \varepsilon_5 dA = \\
 & - \int_A \hat{M}_{11} u_{30,11} dA = - \int_A \hat{M}_{11,11} u_{30} dA + \oint_{S_e} n_1 \hat{M}_{11,1} u_{30} de - \oint_{S_e} n_1 \hat{M}_{11} u_{30,1} de \\
 & \int_A \hat{M}_{22} \varepsilon_6 dA = \\
 & - \int_A \hat{M}_{22} u_{30,22} dA = - \int_A \hat{M}_{22,22} u_{30} dA + \oint_{S_e} n_2 \hat{M}_{22,2} u_{30} de - \oint_{S_e} n_2 \hat{M}_{22} u_{30,2} de \\
 & \int_A \hat{M}_{12} \varepsilon_7 dA = \\
 & - 2 \int_A \hat{M}_{12} u_{30,12} dA = - 2 \int_A \hat{M}_{12,21} u_{30} dA + 2 \oint_{S_e} n_1 \hat{M}_{12,2} u_{30} de - 2 \oint_{S_e} n_2 \hat{M}_{12} u_{30,1} de
 \end{aligned} \tag{25}$$

where  $S_e$  is the boundary counter of the element e,  $n_i$  is the outward norm. The condition of stationarity of  $\Pi_R$  in Eq.(23) leads to:

$$D^{-1} \sigma = \boldsymbol{\varepsilon}^L \tag{26}$$

in each element

$$\begin{aligned}
 & \hat{N}_{11,1} + \hat{N}_{12,2} = 0 \\
 & \hat{N}_{22,2} + \hat{N}_{21,1} = 0 \\
 & \hat{N}_{12} - \hat{N}_{21} = 0 \\
 & \hat{M}_{11,11} + \hat{M}_{22,22} + 2\hat{M}_{21,21} + (N_{11}^0 u_{30,1})_{,1} + (N_{22}^0 u_{30,2})_{,2} \\
 & + \frac{1}{2} [(N_{12}^0 + N_{21}^0) u_{30,1}]_{,2} + \frac{1}{2} [(N_{12}^0 + N_{21}^0) u_{30,2}]_{,1} = 0
 \end{aligned} \tag{27}$$

and the nodal equilibrium equations, which arise out of the term:

$$\begin{aligned}
 & \sum_{elem} \left\{ \int_{S_e} n_1 \hat{N}_{11} \delta u_{10} de + \int_{S_e} n_2 \hat{N}_{22} \delta u_{20} de + \int_{S_e} n_2 \hat{N}_{12} \delta u_{10} de + \int_{S_e} n_1 \hat{N}_{21} \delta u_{20} de \right. \\
 & + \int_{S_e} n_1 \hat{M}_{11,1} \delta u_{30} de - \int_{S_e} n_1 \hat{M}_{11} \delta u_{30,1} de + \int_{S_e} n_2 \hat{M}_{22,2} \delta u_{30} de - \int_{S_e} n_2 \hat{M}_{22} \delta u_{30,2} de \\
 & + 2 \int_{S_e} n_1 \hat{M}_{12,2} \delta u_{30} de - 2 \int_{S_e} n_2 \hat{M}_{12} \delta u_{30,1} de \\
 & + \int_{S_e} n_1 N_{11}^0 u_{30,1} \delta u_{30} de + \int_{S_e} n_2 N_{22}^0 u_{30,2} \delta u_{30} de \\
 & \left. + \frac{1}{2} \int_{S_e} n_2 (N_{12}^0 + N_{21}^0) u_{30,1} \delta u_{30} de + \frac{1}{2} \int_{S_e} n_1 (N_{12}^0 + N_{21}^0) u_{30,2} \delta u_{30} de + \bar{\mathbf{Q}} \delta \mathbf{q} \right\} \\
 & = 0
 \end{aligned} \tag{28}$$

It can be seen that the Reissner functional for von-Karman nonlinear theory of the plate in the current configuration, involves only the variables:

- (1) 4  $N_{\alpha\beta}$  (unsymmetric), and 3  $M_{\alpha\beta}$  (symmetric) in each element.  $N_{\alpha\beta}$  are assumed as being constants, and  $M_{\alpha\beta}$  are assumed to be linear in each element.
- (2) The squares of rotations  $u_{30,\alpha}$  can directly be assumed as being linear in each element [i.e. there is no need to assumed a  $C^1$  continuous  $u_{30}$  directly].
- (3) The drilling degree of freedom  $\theta_3$  in the element, as well as the in plane displacements  $u_{\alpha 0}$  can be assumed to be linear in each element.

These assumptions are discussed in detail below.

### 3.2 Trial functions for $N_{\alpha\beta}; M_{\alpha\beta}; u_{30,\alpha}; \theta_3$ ; and $u_{\alpha 0}$ in each element

We consider the triangular element with three nodes, as shown in Fig.1. The trial functions for  $\sigma$ , in each element, are assumed as

$$\begin{aligned}
 N_{11} &= \beta_1 \\
 N_{22} &= \beta_2 \\
 N_{12} &= \beta_3 \\
 N_{21} &= \beta_4
 \end{aligned}$$

$$\begin{aligned}
 M_{11} &= M_2 = \beta_5 + x\beta_6 + y\beta_7 \\
 M_{22} &= -M_1 = \beta_8 + x\beta_9 + y\beta_{10} \\
 M_{12} &= \beta_{11} + x\beta_{12} + y\beta_{13}
 \end{aligned}
 \tag{29}$$

The matrix form of the Eq.(29) is

$$\boldsymbol{\sigma} = \mathbf{P}\boldsymbol{\beta}
 \tag{30}$$

where

$$\boldsymbol{\beta} = [\beta_1 \ \beta_2 \ \beta_3 \ \cdots \ \beta_{11} \ \beta_{12} \ \beta_{13}]^T
 \tag{31}$$

$$\mathbf{P} = \begin{bmatrix} 1 & 0 & 0 & 0 & 0 & 0 & 0 & 0 & 0 & 0 & 0 & 0 & 0 \\ 0 & 1 & 0 & 0 & 0 & 0 & 0 & 0 & 0 & 0 & 0 & 0 & 0 \\ 0 & 0 & 1 & 0 & 0 & 0 & 0 & 0 & 0 & 0 & 0 & 0 & 0 \\ 0 & 0 & 0 & 1 & 0 & 0 & 0 & 0 & 0 & 0 & 0 & 0 & 0 \\ 0 & 0 & 0 & 0 & 1 & x & y & 0 & 0 & 0 & 0 & 0 & 0 \\ 0 & 0 & 0 & 0 & 0 & 0 & 0 & 1 & x & y & 0 & 0 & 0 \\ 0 & 0 & 0 & 0 & 0 & 0 & 0 & 0 & 0 & 1 & x & y & 0 \end{bmatrix}
 \tag{32}$$

In a same way, the initial stress  $\boldsymbol{\sigma}^0$  can be expressed as

$$\boldsymbol{\sigma}^0 = \mathbf{P}\boldsymbol{\beta}^0
 \tag{33}$$

where

$$\boldsymbol{\beta}^0 = [\beta_1^0 \ \beta_2^0 \ \beta_3^0 \ \cdots \ \beta_{11}^0 \ \beta_{12}^0 \ \beta_{13}^0]^T
 \tag{34}$$

For the second item  $\Pi_{R2}$  in the functional of Eq.(23), only the squares of  $u_{30,1}$  and  $u_{30,2}$  occur within each element. Thus,  $\theta_1 = u_{30,2}$  and  $\theta_2 = -u_{30,1}$  are assumed directly to be linear within each element, in terms of their respective nodal values. This is enormously simple and advantageous in contrast to the primal approach wherein  $u_{30}$  were required to be  $C^1$  continuous over each element, and thus were assumed to be Herimitian polynomials over each element. In this paper, however, we assume:

$$\mathbf{u}_\theta = \begin{Bmatrix} \theta_1 \\ \theta_2 \end{Bmatrix} = \mathbf{N}_\theta \mathbf{a}_\theta = \begin{bmatrix} L_1 & 0 & L_2 & 0 & L_3 & 0 \\ 0 & L_1 & 0 & L_2 & 0 & L_3 \end{bmatrix} \begin{Bmatrix} {}^1\theta_1 \\ {}^1\theta_2 \\ {}^2\theta_1 \\ {}^2\theta_2 \\ {}^3\theta_1 \\ {}^3\theta_2 \end{Bmatrix}
 \tag{35}$$

where  $L_i$  are the area coordinates of the triangular plate elements.  $L_i$  can be expressed as

$$L_i = \frac{1}{2A} (a_i + b_i x_1 + c_i x_2) \tag{36}$$

$$a_i = x_j y_m - x_m y_j$$

$$b_i = y_j - y_m \tag{37}$$

$$c_i = -x_j + x_m$$

where  $A$  is the area of the triangular element,  $x = x_1, y = x_2, (x_i, y_j)$  are the coordinates of the nodes of the element, and  $i = 1, 2, 3; j = 2, 3, 1; k = 3, 1, 2$ .

Assuming that ‘ $\mathbf{a}$ ’ represents the vector of generalized displacements of the nodes of the triangular plate element in the co-rotational updated Lagrangian reference frame  $\mathbf{e}_i$  of Fig.1, the displacement vectors of node  $i$  are:

$$\begin{aligned} {}^i \mathbf{a} &= [{}^i u_1 \quad {}^i u_2 \quad {}^i u_3 \quad {}^i u_4 \quad {}^i u_5 \quad {}^i u_6]^T \\ &= [{}^i u_{10} \quad {}^i u_{20} \quad {}^i u_{30} \quad {}^i \theta_1 \quad {}^i \theta_2 \quad {}^i \theta_3]^T \quad [i = 1, 2, 3] \end{aligned} \tag{38}$$

The relation between  $\mathbf{a}_\theta$  and  $\mathbf{a}$  can be expressed as

$$\mathbf{a}_\theta = \mathbf{T}_\theta \mathbf{a} \tag{39}$$

where

$$\mathbf{T}_\theta = \begin{bmatrix} {}^1 \mathbf{T}_\theta & 0 & 0 \\ 0 & {}^2 \mathbf{T}_\theta & 0 \\ 0 & 0 & {}^3 \mathbf{T}_\theta \end{bmatrix} \tag{40}$$

$${}^i \mathbf{T}_\theta = \begin{bmatrix} 0 & 0 & 0 & 1 & 0 & 0 \\ 0 & 0 & 0 & 0 & 1 & 0 \end{bmatrix} \tag{41}$$

For the third item  $\Pi_{R3}$  in the functional of Eq.(23), the trial functions for the displacements along the boundary of the element, for instance, on boundary 1-2 in Fig.3, are separately chosen as

$${}^{(1)} \mathbf{u}_b = \begin{Bmatrix} {}^{(1)} u_{10} \\ {}^{(1)} u_{20} \\ {}^{(1)} u_{30} \\ {}^{(1)} \theta_s \end{Bmatrix} = {}^{(1)} \mathbf{N}_b {}^{(1)} \mathbf{a} = [{}^1 \mathbf{N}_b \quad {}^2 \mathbf{N}_b] \begin{Bmatrix} {}^1 \mathbf{b} \\ {}^2 \mathbf{b} \end{Bmatrix} \tag{42}$$

where

$${}^i \mathbf{b} = [{}^i u_{10} \quad {}^i u_{20} \quad {}^i u_{30} \quad {}^i \theta_s \quad {}^i \theta_n]^T \tag{43}$$

$${}^i\mathbf{N}_b = \begin{bmatrix} \phi_i & 0 & 0 & 0 & 0 \\ 0 & \phi_i & 0 & 0 & 0 \\ 0 & 0 & H_i^0 & 0 & -H_i^1 \\ 0 & 0 & 0 & \phi_i & 0 \end{bmatrix} \quad (44)$$

$$\begin{aligned} \phi_1 &= 1 - \xi, \phi_2 = \xi, \\ H_1^0 &= 1 - 3\xi^2 + 2\xi^3, H_1^1 = d_1 (\xi - 2\xi^2 + \xi^3) \\ H_2^0 &= 3\xi^2 - 2\xi^3, H_2^1 = -d_1 (\xi^2 - \xi^3) \end{aligned} \quad (45)$$

where  $\theta_s = \partial u_{30} / \partial n, \theta_n = -\partial u_{30} / \partial s$ ,  $d_1$  is the length of boundary 1-2 and  $\xi = s/d_1$ .

The relation between  $(\theta_s, \theta_n)$  and  $(\theta_1, \theta_2)$  on boundary 1-2 in Fig.3 can be expressed as

$$\begin{Bmatrix} \theta_s \\ \theta_n \end{Bmatrix} = \begin{bmatrix} \cos \alpha & \sin \alpha \\ -\sin \alpha & \cos \alpha \end{bmatrix} \begin{Bmatrix} \theta_1 \\ \theta_2 \end{Bmatrix} \quad (46)$$

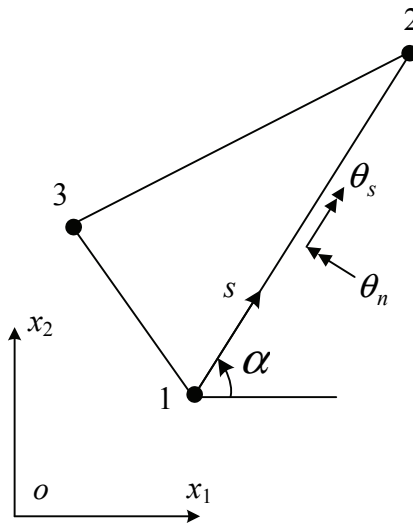


Figure 3: Triangular plate element

The stresses  ${}^{(1)}\boldsymbol{\sigma}$  along the boundary can be obtained by using Eq.(29), along with the expressions of

$$\begin{cases} x = x_1 + c_3 \xi \\ y = y_1 - b_3 \xi \end{cases} \quad (47)$$

where  $b_3$  and  $c_3$  are defined in Eq.(37).

Similarly, other trial functions  $^{(i)}\mathbf{u}_b$  ( $i = 2, 3$ ) and  $^{(i)}\boldsymbol{\sigma}$  along the boundary of the element can be obtained by cyclic permutation.

The drilling degrees  $\theta_3$  are also assumed directly to be linear within each element in a same way of  $\theta_1$  and  $\theta_2$  in Eq.(35).

### 3.3 Explicit expressions of the tangent stiffness matrix for each element

Because of the assumption of the trial functions of the stresses in Eq.(29), the following items in Eq.(25) become

$$\begin{aligned} \int_A \hat{N}_{11,1} u_{10} dA &= 0, \int_A \hat{N}_{22,2} u_{20} dA = 0, \int_A \hat{N}_{12,2} u_{10} dA = 0, \\ \int_A \hat{N}_{21,1} u_{20} dA &= 0, \int_A \hat{M}_{11,11} u_{30} dA = 0, \int_A \hat{M}_{22,22} u_{30} dA = 0, \\ \int_A \hat{M}_{12,21} u_{30} dA &= 0 \end{aligned} \quad (48)$$

Thus, Eq.(24) can be rewritten as

$$\Pi_{R1} = \frac{1}{2} \int_A (\boldsymbol{\sigma}^T \mathbf{D}^{-1} \boldsymbol{\sigma}) dA = \frac{1}{2} \int_A (\boldsymbol{\beta}^T \mathbf{P}^T \mathbf{C} \mathbf{P} \boldsymbol{\beta}) dA \quad (49)$$

$$\begin{aligned} \Pi_{R2} &= \frac{1}{2} \int_A [N_{11}^0 u_{30,1}^2 + N_{22}^0 u_{30,2}^2 + (N_{12}^0 + N_{21}^0) u_{30,1} u_{30,2}] dA \\ &= \frac{1}{2} \int_A [N_{11}^0 \theta_2^2 + N_{22}^0 \theta_1^2 - (N_{12}^0 + N_{21}^0) \theta_1 \theta_2] dA \\ &= \frac{1}{2} \int_A \mathbf{u}_\theta^T \boldsymbol{\sigma}_\theta^0 \mathbf{u}_\theta dA = \frac{1}{2} \int_A \mathbf{a}^T \mathbf{T}_\theta^T \mathbf{N}_\theta^T \boldsymbol{\sigma}_\theta^0 \mathbf{N}_\theta \mathbf{T}_\theta \mathbf{a} dA \end{aligned} \quad (50)$$

where

$$\boldsymbol{\sigma}_\theta^0 = \begin{bmatrix} N_{22}^0 & -N_{12}^0 \\ -N_{21}^0 & N_{11}^0 \end{bmatrix} \quad (51)$$

in  $\Pi_{R2}$ , only the squares of  $u_{30,1}$  and  $u_{30,2}$  appear within each element. Thus,  $\theta_1 = u_{30,2}$  and  $\theta_2 = -u_{30,1}$  are simply assumed to be  $C^0$  continuous within each element.

Letting  $\mathbf{A}_{mn} = \mathbf{T}_\theta^T \mathbf{N}_\theta^T \mathbf{N}_\theta \mathbf{T}_\theta$ ,  $\Pi_{R2}$  can be rewritten as

$$\Pi_{R2} = \frac{1}{2} \int_A \mathbf{a}^T \mathbf{A}_{mn} \mathbf{a} dA \quad (52)$$

$$\begin{aligned}
 \Pi_{R3} &= \oint_{S_e} n_1 \hat{N}_{11} u_{10} de + \oint_{S_e} n_2 \hat{N}_{22} u_{20} de + \oint_{S_e} n_2 \hat{N}_{12} u_{10} de + \oint_{S_e} n_1 \hat{N}_{21} u_{20} de \\
 &+ \oint_{S_e} n_1 \hat{M}_{11,1} u_{30} de - \oint_{S_e} n_1 \hat{M}_{11} u_{30,1} de + \oint_{S_e} n_2 \hat{M}_{22,2} u_{30} de - \oint_{S_e} n_2 \hat{M}_{22} u_{30,2} de \\
 &+ 2 \oint_{S_e} n_1 \hat{M}_{12,2} u_{30} de - 2 \oint_{S_e} n_2 \hat{M}_{12} u_{30,1} de + \int_A \hat{N}_{12} \theta_3 dA - \int_A \hat{N}_{21} \theta_3 dA \\
 &= (\boldsymbol{\beta} + \boldsymbol{\beta}^0)^T \mathbf{R}_\sigma \mathbf{a}
 \end{aligned} \tag{53}$$

where  $\mathbf{R}_\sigma$  is a  $13 \times 18$  constant matrix, and can be explicitly expressed with the coordinates of the nodes of the triangular element, by using the trial functions in Eqs. (29), (35) and (42). Please see the Matlab codes at the appendix for obtaining the explicit expression of the matrix  $\mathbf{R}_\sigma$ .

$$\Pi_{R4} = \mathbf{a}^T \mathbf{F} \tag{54}$$

By invoking  $\delta \Pi_R = 0$ , we can obtain

$$\begin{aligned}
 \delta \Pi_R &= \sum_{elem} \delta \boldsymbol{\beta}^T \left\{ - \int_A \mathbf{P}^T \mathbf{C} \mathbf{P} \boldsymbol{\beta} dA + \mathbf{R}_\sigma \mathbf{a} \right\} + \\
 &\sum_{elem} \delta \mathbf{a}^T \left\{ \mathbf{R}_\sigma^T \boldsymbol{\beta} + \int_A \mathbf{A}_{nm} \mathbf{a} dA + \mathbf{R}_\sigma^T \boldsymbol{\beta}^0 - \mathbf{F} \right\}
 \end{aligned} \tag{55}$$

Let

$$\mathbf{H} = \int_A \mathbf{P}^T \mathbf{C} \mathbf{P} dA, \mathbf{G} = \mathbf{R}_\sigma, \mathbf{K}_N = \int_A \mathbf{A}_{nm} dA, \mathbf{F}^0 = \mathbf{G}^T \boldsymbol{\beta}^0 \tag{56}$$

then

$$\delta \Pi_R = \sum_{elem} \delta \boldsymbol{\beta}^T \{ -\mathbf{H} \boldsymbol{\beta} + \mathbf{G} \mathbf{a} \} - \sum_{elem} \delta \mathbf{a}^T \{ \mathbf{G}^T \boldsymbol{\beta} + \mathbf{K}_N \mathbf{a} - \mathbf{F} + \mathbf{F}^0 \} = 0 \tag{57}$$

Since  $\delta \boldsymbol{\beta}^T$  in Eq.(57) are independent and arbitrary in each element, one obtains

$$\boldsymbol{\beta} = \mathbf{H}^{-1} \mathbf{G} \mathbf{a} \tag{58}$$

and

$$\sum_{elem} \delta \mathbf{a}^T \{ (\mathbf{K}_L + \mathbf{K}_N) \mathbf{a} - \mathbf{F} + \mathbf{F}^0 \} = 0 \tag{59}$$

where

$$\mathbf{K}_L = \mathbf{G}^T \mathbf{H}^{-1} \mathbf{G} \tag{60}$$

$$\mathbf{K}_N = \int_A \mathbf{A}_{nn} dA \tag{61}$$

The components of the element tangent stiffness matrix,  $\mathbf{K}_L$  and  $\mathbf{K}_N$ , respectively, can be derived explicitly after some simple algebra.  $\mathbf{K}_L$  is the usual linear symmetric ( $18 \times 18$ ) stiffness matrix of the plate in the co-rotational reference frame and can be explicitly expressed by using  $\mathbf{H}$  in Eq.(56) and  $\mathbf{G} = \mathbf{R}_\sigma$  which is obtained at the appendix. However, the nonlinear stiffness matrix  $\mathbf{K}_N$  is asymmetric ( $18 \times 18$ ) stiffness matrix because of the introduction of the drilling degrees of freedom. In Eq.(60),  $\mathbf{H}$  is a ( $13 \times 13$ ) matrix, and  $\mathbf{G}$  is a ( $13 \times 18$ ) matrix. The number of stress parameters ( $n_\sigma$ ) in the development of the present element is 13, the number of displacement coordinates ( $n_q$ ) for the element is 18, and the number of rigid-body modes ( $n_\pi$ ) for the element is 6. Thus, as shown in Xue, Karlovitz and Atluri (1985), the necessary condition for satisfying the element stability [LBB] condition, namely,  $n_\sigma \geq n_q - n_\pi$  is satisfied. Furthermore, it has been verified that the present element does not possess any Kinematic (zero-energy) deformation modes. It is clear from the above procedures, that the present ( $18 \times 18$ ) tangent stiffness matrices of the plate in the co-rotational reference frame, based on the Reissner variational principle and von Karman type strains, are very simple and can be explicitly derived.

**4 Transformation between deformation dependent co-rotational local base vectors  $[\mathbf{e}_i]$ , and the global  $[\bar{\mathbf{e}}_i]$  frames of reference**

As shown in Fig.1,  $\bar{x}_i$  ( $i = 1, 2, 3$ ) are the global coordinates with unit basis vectors  $\bar{\mathbf{e}}_i$ . By letting  $x_i$  and  $\mathbf{e}_i$  be the co-rotational reference coordinates for the deformed plate element, the basis vectors  $\mathbf{e}_i$  are chosen such that

$$\begin{aligned} \mathbf{e}_1 &= (\boldsymbol{\chi}_0^2 - \boldsymbol{\chi}_0^1) / \|\boldsymbol{\chi}_0^2 - \boldsymbol{\chi}_0^1\| \\ \mathbf{e}_{13} &= (\boldsymbol{\chi}_0^3 - \boldsymbol{\chi}_0^1) / \|\boldsymbol{\chi}_0^3 - \boldsymbol{\chi}_0^1\| \\ \mathbf{e}_3 &= (\mathbf{e}_1 \times \mathbf{e}_{13}) / \|\mathbf{e}_1 \times \mathbf{e}_{13}\| \\ \mathbf{e}_2 &= \mathbf{e}_3 \times \mathbf{e}_1 \end{aligned}$$

where  $\boldsymbol{\chi}_0^i$  ( $i = 1, 2, 3$ ) are the position vectors of the nodes 1,2,3 respectively of the element in the current reference state, in the global Cartesian frame  $[\boldsymbol{\chi}_0^i = \bar{x}_j^i \bar{\mathbf{e}}_j]$ .

Thus, we find

$$\begin{aligned} \mathbf{e}_1 &= (\bar{x}_1^{12} \bar{\mathbf{e}}_1 + \bar{x}_2^{12} \bar{\mathbf{e}}_2 + \bar{x}_3^{12} \bar{\mathbf{e}}_3) / l^{12} = \tilde{a}_1 \bar{\mathbf{e}}_1 + \tilde{a}_2 \bar{\mathbf{e}}_2 + \tilde{a}_3 \bar{\mathbf{e}}_3 \\ \mathbf{e}_3 &= \tilde{c}_1 \bar{\mathbf{e}}_1 + \tilde{c}_2 \bar{\mathbf{e}}_2 + \tilde{c}_3 \bar{\mathbf{e}}_3 \\ \mathbf{e}_2 &= \mathbf{e}_3 \times \mathbf{e}_1 \end{aligned} \tag{62}$$

where  $\bar{x}_i^{jk} = \bar{x}_i^j - \bar{x}_i^k$ ,  $l^{jk} = \left[ (\bar{x}_1^{jk})^2 + (\bar{x}_2^{jk})^2 + (\bar{x}_3^{jk})^2 \right]^{\frac{1}{2}}$ ,

$$\tilde{b}_1 = \frac{\bar{x}_1^{13}}{l^{13}}, \quad \tilde{b}_2 = \frac{\bar{x}_2^{13}}{l^{13}}, \quad \tilde{b}_3 = \frac{\bar{x}_3^{13}}{l^{13}} \tag{63}$$

$$\tilde{c}_1 = \frac{\tilde{a}_2 \tilde{b}_3 - \tilde{a}_3 \tilde{b}_2}{l^c}, \quad \tilde{c}_2 = \frac{\tilde{a}_3 \tilde{b}_1 - \tilde{a}_1 \tilde{b}_3}{l^c}, \quad \tilde{c}_3 = \frac{\tilde{a}_1 \tilde{b}_2 - \tilde{a}_2 \tilde{b}_1}{l^c} \tag{64}$$

and

$$l^c = \left[ (\tilde{a}_2 \tilde{b}_3 - \tilde{a}_3 \tilde{b}_2)^2 + (\tilde{a}_3 \tilde{b}_1 - \tilde{a}_1 \tilde{b}_3)^2 + (\tilde{a}_1 \tilde{b}_2 - \tilde{a}_2 \tilde{b}_1)^2 \right]^{\frac{1}{2}} \tag{65}$$

Then  $\mathbf{e}_i$  and  $\bar{\mathbf{e}}_i$  have the following relations:

$$\begin{Bmatrix} \mathbf{e}_1 \\ \mathbf{e}_2 \\ \mathbf{e}_3 \end{Bmatrix} = \begin{bmatrix} \tilde{a}_1 & \tilde{a}_2 & \tilde{a}_3 \\ \tilde{d}_1 & \tilde{d}_2 & \tilde{d}_3 \\ \tilde{c}_1 & \tilde{c}_2 & \tilde{c}_3 \end{bmatrix} \begin{Bmatrix} \bar{\mathbf{e}}_1 \\ \bar{\mathbf{e}}_2 \\ \bar{\mathbf{e}}_3 \end{Bmatrix} \tag{66}$$

where

$$\tilde{d}_1 = \tilde{c}_2 \tilde{a}_3 - \tilde{c}_3 \tilde{a}_2, \quad \tilde{d}_2 = \tilde{c}_3 \tilde{a}_1 - \tilde{c}_1 \tilde{a}_3, \quad \tilde{d}_3 = \tilde{c}_1 \tilde{a}_2 - \tilde{c}_2 \tilde{a}_1 \tag{67}$$

$$\boldsymbol{\lambda}_0 = \begin{bmatrix} \tilde{a}_1 & \tilde{a}_2 & \tilde{a}_3 \\ \tilde{d}_1 & \tilde{d}_2 & \tilde{d}_3 \\ \tilde{c}_1 & \tilde{c}_2 & \tilde{c}_3 \end{bmatrix} \tag{68}$$

Thus, the transformation matrix  $\boldsymbol{\lambda}$  for the plate element, between the 18 generalized coordinates in the co-rotational reference frame  $\mathbf{e}_i$ , and the corresponding 18 coordinates in the global Cartesian reference frame  $\bar{\mathbf{e}}_i$ , is given by

$$\boldsymbol{\lambda} = \begin{bmatrix} \boldsymbol{\lambda}_0 & 0 & 0 & 0 & 0 & 0 \\ 0 & \boldsymbol{\lambda}_0 & 0 & 0 & 0 & 0 \\ 0 & 0 & \boldsymbol{\lambda}_0 & 0 & 0 & 0 \\ 0 & 0 & 0 & \boldsymbol{\lambda}_0 & 0 & 0 \\ 0 & 0 & 0 & 0 & \boldsymbol{\lambda}_0 & 0 \\ 0 & 0 & 0 & 0 & 0 & \boldsymbol{\lambda}_0 \end{bmatrix} \tag{69}$$

Then the element matrices are transformed to the global coordinate system using

$$\bar{\mathbf{a}} = \boldsymbol{\lambda}^T \mathbf{a} \tag{70}$$

$$\bar{\mathbf{K}} = \boldsymbol{\lambda}^T \mathbf{K} \boldsymbol{\lambda} \tag{71}$$

$$\bar{\mathbf{F}} = \boldsymbol{\lambda}^T \mathbf{F} \tag{72}$$

where  $\bar{\mathbf{a}}$ ,  $\bar{\mathbf{K}}$ ,  $\bar{\mathbf{F}}$  are respectively the generalized nodal displacements, element tangent stiffness matrix and generalized nodal forces, in the global coordinates system. The Newton-Raphson method is used to solve the nonlinear equation of the plate in this implementation.

## 5 Numerical examples

### 5.1 Buckling of the thin plate

The  $(18 \times 18)$  tangent stiffness matrix for a plate in space should be capable of predicting buckling under compressive axial loads, when such an axial load interacts with the transverse displacement in the plate. We consider the plate with two types of boundary conditions as shown in Figs.4a and 4b. Assume that the thickness of the plate is  $h = 0.01$ , and  $a = b = D = 1$ . The buckling loads of the plate obtained by the present method using different numbers of elements are shown in Tab.1. It is seen that the buckling load predicted by the present method agrees well with the analytical solution (buckling load is  $P_{cr} = k\pi^2 D/b^2$ , where  $k = 4$  for Fig.4a and  $k = 1.7$  for Fig.4b).

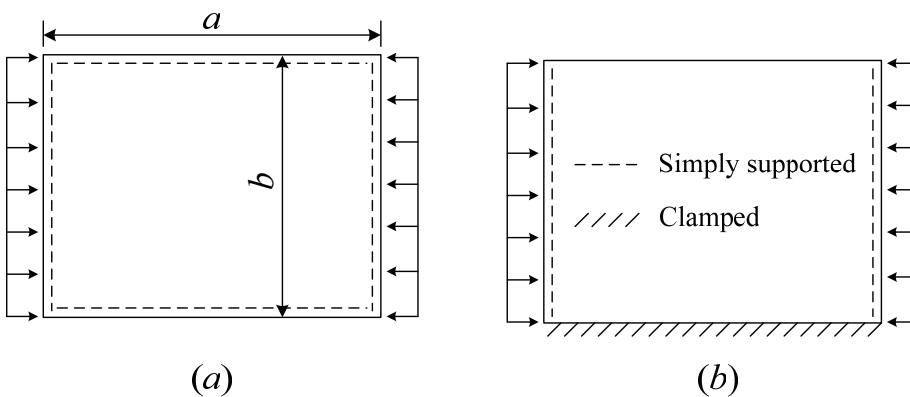


Figure 4: Model of the plate subject to an axial force

Table 1: Buckling load of the plate

Mesh	Fig.4a		Fig.4b	
	Present method	Exact	Present method	Exact
2×2	38.2754	39.4784	18.7710	16.7783
4×4	40.6186		17.4856	
8×8	39.7162		16.9512	
16×16	39.5189		16.8084	

### 5.2 A simply supported or clamped square plate

A simply supported or clamped square plate loaded by a central point load  $P$  or a uniform load  $q$  is considered for linear elastic analysis. The side length and the thickness of the square plate are  $l$  and  $h$ . The results listed in Tab.2 and Tab.3 indicate the good accuracy and convergence rate of the present elements.

Table 2: Central deflection for a square plate clamped along all four boundaries

Mesh	Uniform load ( $w_c \times ql^4/100D$ )	Point load ( $w_c \times Pl^2/100D$ )
2×2	0.0521	0.2083
4×4	0.1148	0.4808
8×8	0.1237	0.5383
16×16	0.1259	0.5548
Exact	0.1260	0.5600

Table 3: Central deflection for a square plate simply supported along all four boundaries

Mesh	Uniform load ( $w_c \times ql^4/100D$ )	Point load ( $w_c \times Pl^2/100D$ )
2×2	0.2417	0.9667
4×4	0.3649	1.0940
8×8	0.3959	1.1406
16×16	0.4037	1.1545
Exact	0.4062	1.1160

**5.3 Geometrically nonlinear analysis of a clamped square plate subjected to a uniform load**

The geometrically nonlinear analysis of a clamped plate under uniform load  $q$  is studied. The side length and the thickness of the square plate are  $l = 100mm$  and  $h = 1mm$ . The material properties are  $E = 2.1e06N/mm^2$  and  $\nu = 0.316$ . The analytic central solution of the plate is given by chia (1980):

$$\left(\frac{w_0}{h}\right)^3 + 0.2522\frac{w_0}{h} = 0.0001333\frac{ql^4}{Dh} \tag{73}$$

where  $w_c = 2.5223w_0$ .

The whole plate is modeled and the central deflection  $w_c$  of the plate for different meshes is shown in Tab.4. It is observed that the results of the present method converge quickly to the analytic solution.

Table 4: The central deflection of a clamped square plate subjected to a uniform load

Mesh	$q$				
	0.5	1.3	2.1	3.4	5.5
2×2	0.133382	0.337638	0.522149	0.775787	1.092368
4×4	0.287872	0.664287	0.938416	1.258908	1.617062
8×8	0.306773	0.681918	0.939928	1.234652	1.561745
Analytical	0.322050	0.688258	0.933327	1.214635	1.531733

**5.4 Geometrically nonlinear analysis of a clamped circular plate subjected to a uniform load**

The large deformation analysis of a clamped circular plate subjected to a uniformly distributed load  $q$  is considered. The radius of the plate is  $r = 100$  and the thickness of the plate is  $h = 2$ . The material properties are  $E = 1.0e07$  and  $\nu = 0.3$ . The analytic central deflection  $w_0$  of the plate is given by Chia (1980):

$$\frac{16}{3(1-\nu^2)} \left[ \frac{w_0}{h} + \frac{1}{360} (1+\nu) (173-73\nu) \left(\frac{w_0}{h}\right)^3 \right] = \frac{qR^4}{Eh^4} \tag{74}$$

Due to the double symmetry, only one quarter of the plate is discretized as shown in Fig.5. Fig.6 shows the comparison of the present result of the central deflection and the analytic solution by Chia (1980). It is observed that the present result is in very good agreement with the analytical solution.

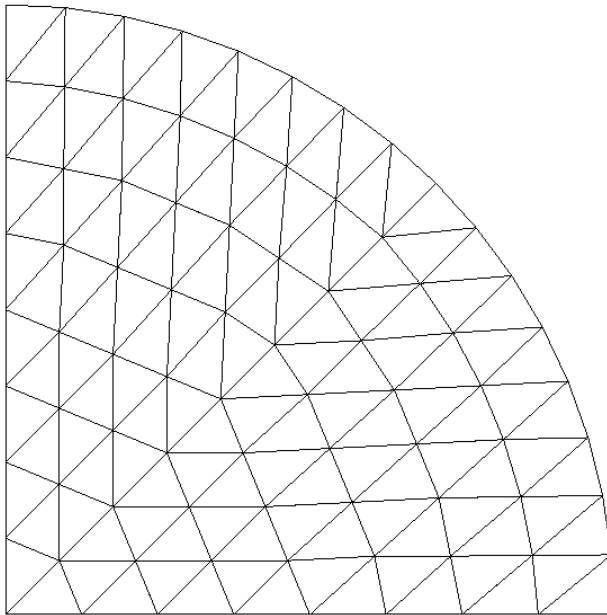


Figure 5: Mesh of one quarter of a clamped circular plate

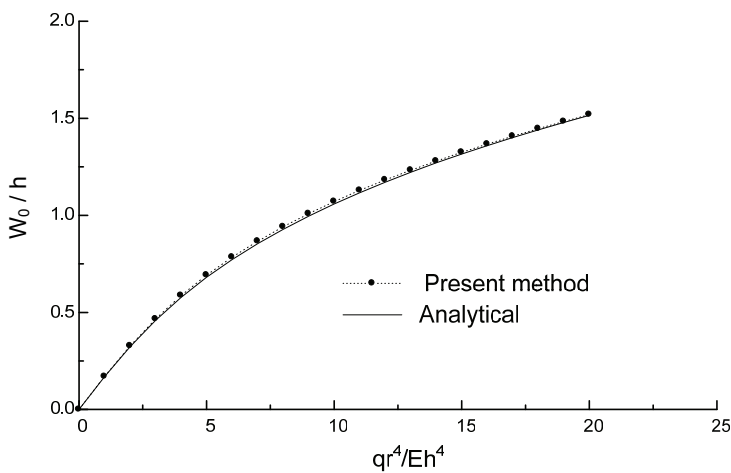


Figure 6: Nonlinear results of a clamped circular plate

### 5.5 Geometrically nonlinear analysis of a clamped circular plate subjected to a concentrated load

The circular plate subjected to a concentrated load  $p$  at the center of the plate is considered (Zhang and Cheung 2003). The geometric and material property are the

same as the Section 5.4. Tab.5 gives the nondimensional central deflections  $w/h$  of the circular plate from the present method and the analytical solution by Chia (1980).

Table 5: Nondimensional central deflection  $w/h$  of a clamped circular plate subjected to a concentrated load

	$pr^2/(Eh^4)$					
	1	2	3	4	5	6
Present method	0.2120	0.4043	0.5704	0.7130	0.8369	0.9465
Analytical solution	0.2129	0.4049	0.5695	0.7098	0.8309	0.9372

**5.6 Large rotations of a plate subject to an end-moment and a transverse load**

A plate subject to an end moment  $M^* = \frac{6Ma}{\pi Ebh^3}$  as shown in Fig.7, is considered (Oral and Barut 1991). The thickness of the plate is  $h = 0.01$ . The widths of the plate are  $a = 8$  and  $b = 1$ . The plate is divided into 16 triangular elements (Fig.7). When  $M^* = 1$ , the plate is almost curled into a complete circle as shown in Fig.8 and the solutions are in good agreement with the analytical solution.

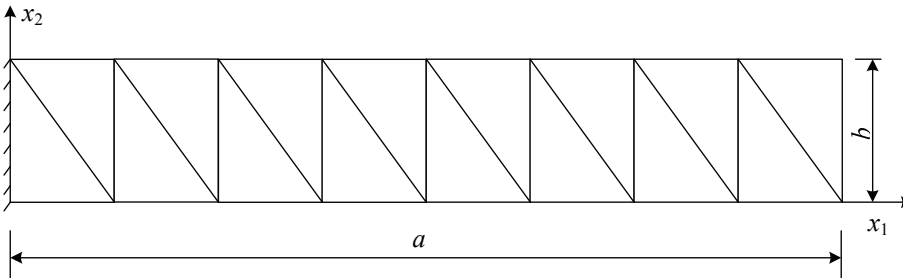


Figure 7: Model for a plate subject to an end-moment

If a non-conservative, follower-type transverse load  $P^* = \frac{6Pa^2}{\pi Ebh^3}$  is applied at the tip, instead of  $M^*$ , the initial and deformed geometries of the cantilever are shown in Fig.9.

**5.7 Nonlinear analysis of a cantilever plate with conservative end load**

The cantilever plate with conservative end load shown in Fig.10 has been analyzed. The geometry parameters are  $a = 40m$ ,  $b = 30m$  and  $h = 0.4m$ . The material properties are  $E = 1.2e8N/m^2$  and  $\nu = 0.3$ . The load-deflection curve is shown in Fig.11

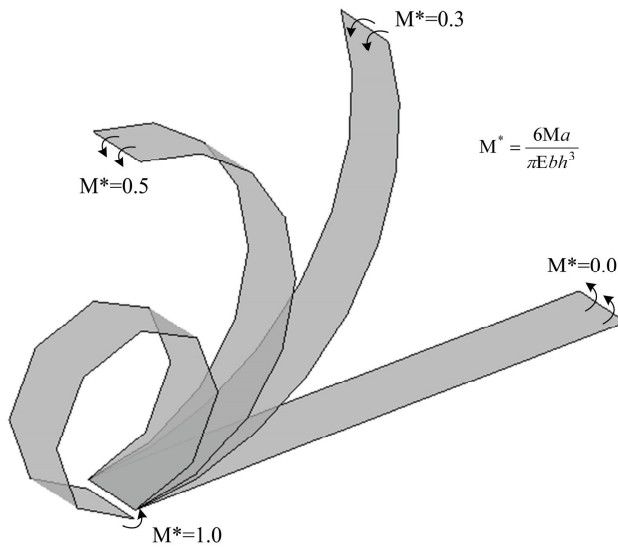


Figure 8: Initial and deformed geometries for the plate subject to an end-moment along  $x_2 = 0$

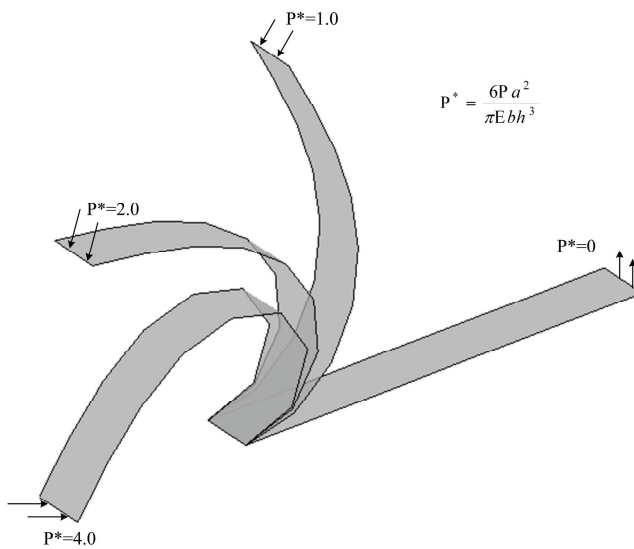


Figure 9: Initial and deformed geometries for the plate subject to a transverse load

where the present solution is compared with the solution by Oral and Barut (1991).  $W_A$  and  $W_B$  in Fig.11 are correspondingly the deflections of point A and point B along  $x_3$ .

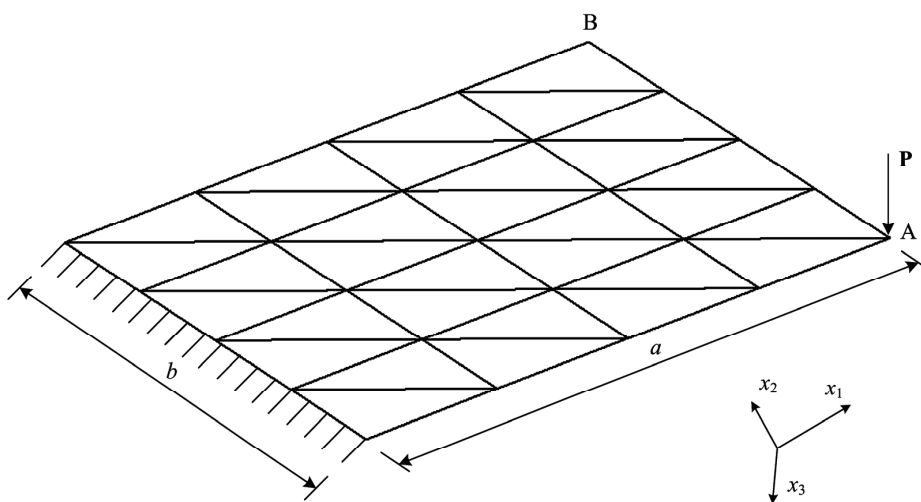


Figure 10: Cantilever plate with end load

### 5.8 Nonlinear analysis of a cylindrical shell panel

A cylindrical shell panel clamped along all four boundaries shown in Fig.12 is considered for nonlinear analysis. The shell panel is subjected to inward radial uniform load  $q$ . The geometry parameters are  $l = 254mm$ ,  $r = 2540mm$ ,  $h = 3.175mm$  and  $\theta = 0.1rad$ . The material properties are  $E = 3.10275kN/mm^2$  and  $\nu = 0.3$ . Due to the double symmetry, only one quarter of the panel is discretized using a mesh of  $8 \times 8$ . The present results of the central deflection together with solutions by Dhatt (1970) are shown in Fig.13. It is observed that the present method works very well.

### 5.9 Hinged spherical shell with central point load

The hemispherical shell with an  $18^\circ$  hole shown in Fig.14 is analyzed. The geometry parameters are the radius  $r = 10m$  and  $h = 0.04m$ . The material properties are  $E = 6.825e7kN/m^2$  and  $\nu = 0.3$ . Due to the double symmetry, only one quarter of the shell is discretized using a mesh of  $8 \times 8$  (Fig.15). Fig.16 shows the present solutions are results are in good agreement with the results of Kim and Lomboy

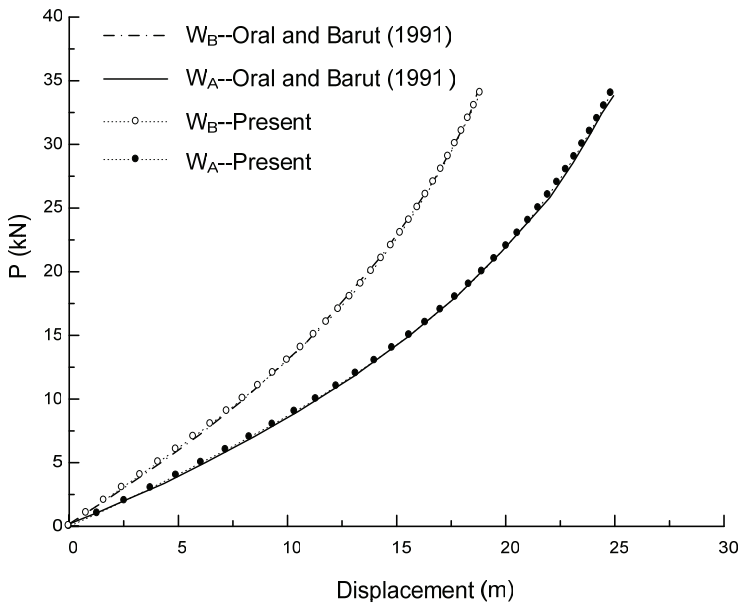


Figure 11: Load-deflection curve for the cantilever plate

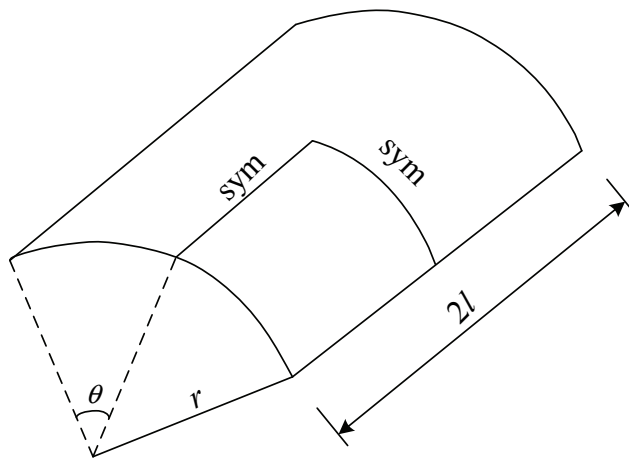


Figure 12: Model of the shell panel

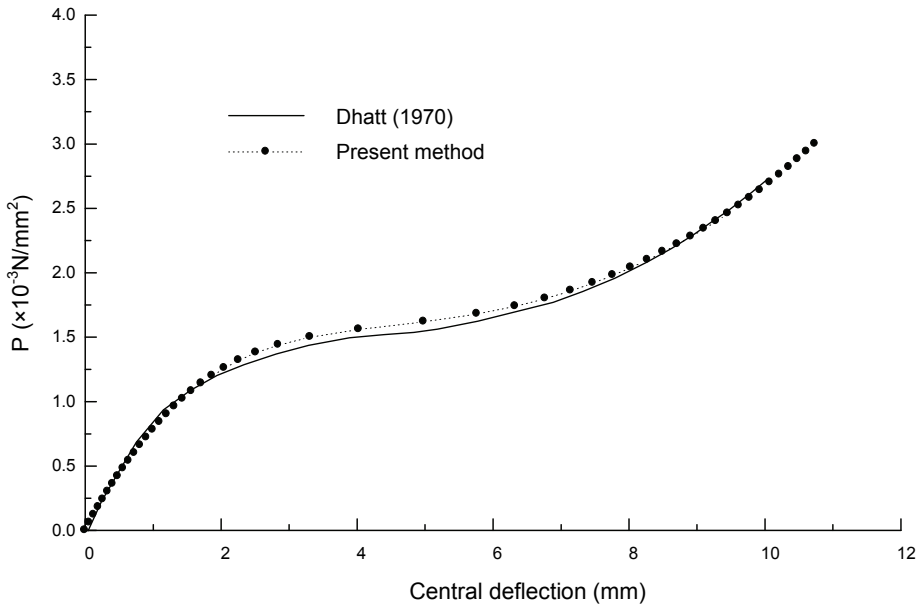


Figure 13: Nonlinear results of a clamped cylindrical shell panel

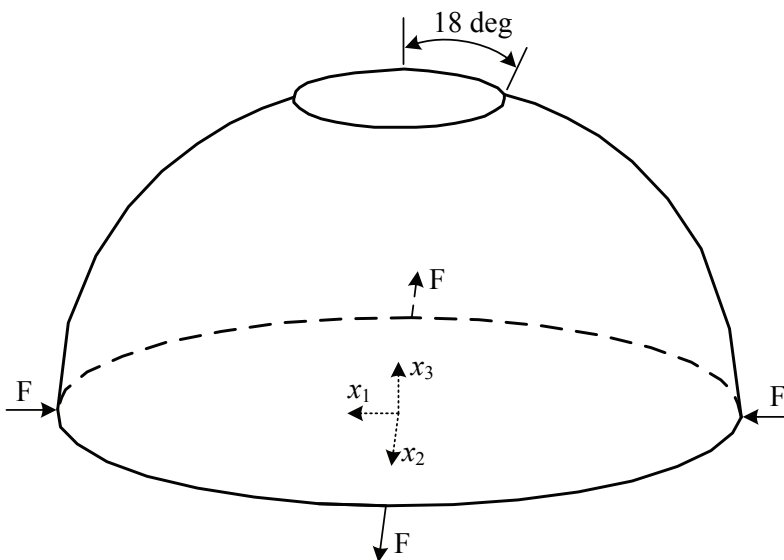


Figure 14: Model for hemispherical shell with an 18<sup>0</sup> hole

(2006) using a mesh of  $8 \times 8$ . The deformed shape of hemispherical shell with a mesh of  $16 \times 16$  when  $F = 200kN$  is shown in Fig.17.

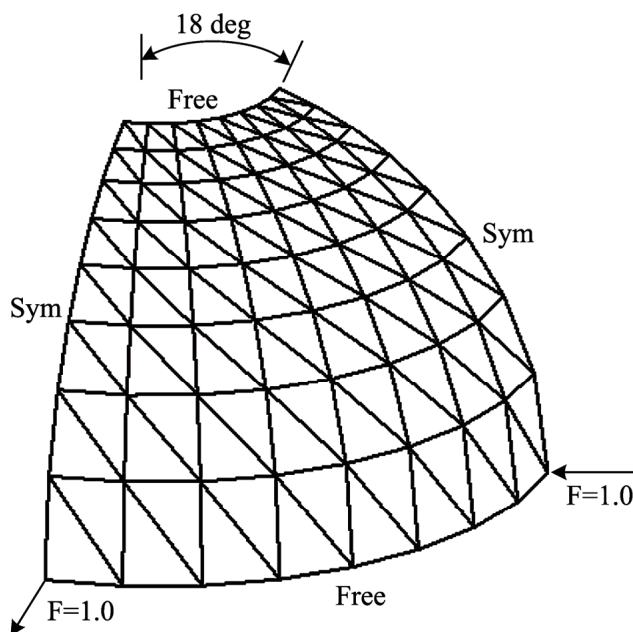


Figure 15: Mesh for the hemispherical shell with an  $18^\circ$  hole

## 6 Conclusions

Based on the Reissner variational principle and a von Karman nonlinear theory of deformation in the updated Lagrangian co-rotational reference frame, a simple finite element method has been developed for large deformation/rotation analyses of plate/shell structures with thin members. The drilling degrees of freedom are introduced as additional variables to avoid the problem of singularity in the stiffness matrix for the large deformation and rotation analyses of the plate/shell structures. The trial functions for the derivatives of transverse displacements and the bending moments can be simply assumed to be linear within each element in the current approach. Thus the development of the present element based on the Reissner's principle is much simpler than the plate/shell element based on the primal method. The explicit expressions for the  $(18 \times 18)$  tangent stiffness matrix of each element can be seen to be derived, in an elementary way, for the geometrically nonlinear analyses of the plate/shell structures. Numerical examples demonstrate that the present

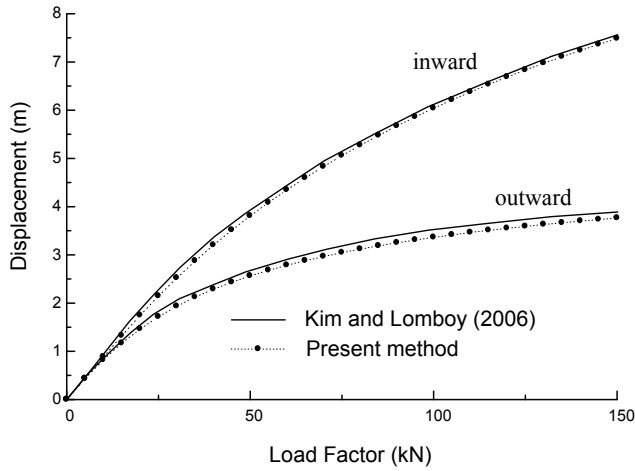


Figure 16: Nonlinear solutions for hemispherical shell

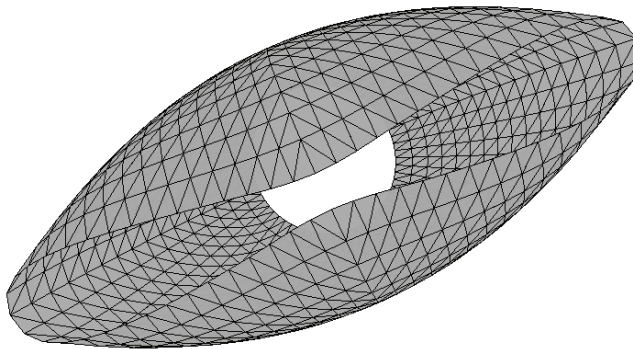


Figure 17: Deformed shape of hemispherical shell when  $F = 200kN$

method is just as competitive, if not more so, as the existing methods, based on the complicated mathematical theories of differential geometry and group-theoretical considerations of finite rotations, in terms of accuracy and efficiency.

**Acknowledgement:** The authors gratefully acknowledge the support of the Nature Science Foundation of China (NSFC, 10972161) and the support of Kwang-Hua Fund for College of Civil Engineering, Tongji University. At UCI, this research was supported by the Army Research Office, with Dr. Larry Russell as the Program official. This research was also supported by the World Class University

(WCU) program through the National Research Foundation of Korea funded by the Ministry of Education, Science and Technology (Grant no.: R33-10049). The second author is also pleased to acknowledge the support of The Lloyd's Register Educational Trust (The LRET) which is an independent charity working to achieve advances in transportation, science, engineering and technology education, training and research worldwide for the benefit of all.

## References

- Allman, D.J.** (1988): A quadrilateral finite element including vertex rotations for plane elasticity problems. *International Journal for Numerical Methods in Engineering*, Vol.26, pp. 717-739.
- Atluri, S.N.** (1975): On 'hybrid' finite element models in solid mechanics, Advances in computer methods for partial differential equations, R. Vichrevetsky, Ed., AICA, pp. 346-355.
- Atluri, S.N.** (1979): On rate principles for finite strain analysis of elastic and inelastic nonlinear solids, Recent research on mechanical behavior, University of Tokyo Press, pp. 79-107.
- Atluri, S.N.** (1980): On some new general and complementary energy theorems for the rate problems in finite strain, classical elastoplasticity. *Journal of Structural Mechanics*, Vol. 8(1), pp. 61-92.
- Atluri, S.N.** (1984): Alternate stress and conjugate strain measures, and mixed variational formulations involving rigid rotations, for computational analyses of finitely deformed plates and shells: part-I: theory. *Computers & Structures*, Vol. 18(1), pp. 93-116.
- Atluri, S.N.; Cazzani, A.** (1994): Rotations in computational solid mechanics, invited feature article. *Archives for Computational Methods in Engg.*, ICNME, Barcelona, Spain, Vol 2(1), pp. 49-138.
- Atluri, S. N.; Gallagher, R. H.; Zienkiewicz, O. C. (Editors).** (1983): Hybrid & Mixed Finite Element Methods, J. Wiley & Sons, 600 pages.
- Atluri, S.N.; Murakawa, H.** (1977): On hybrid finite element models in nonlinear solid mechanics, finite elements in nonlinear mechanics, P.G. Bergan et al, Eds., Tapir Press, Norway, Vol. 1, pp. 3-40.
- Atluri, S.N.; Reissner, E.** (1989): On the formulation of variational theorems involving volume constraints. *Computational Mechanics*, Vol. 5, pp 337-344.
- Chia, C.Y.** (1980): Nonlinear Analysis of Plate. McGraw-Hill, New York.
- Crisfield, M.A.** (1990): A consistent co-rotational formulation for non-linear, three-dimensional, beam-elements. *Computer Methods in Applied Mechanics and Engi-*

*neering*, Vol.81, pp. 131–150.

**Dhatt, G.S.** (1970): Instability of thin shells by the finite element method. IASS Symposium for Folded Plates and Prismatic Structures, Vienna.

**Huang, B.Z.; Shenoy, V.B.; Atluri, S.N.** (1994): A quasi-conforming triangular laminated composite shell element based on a refined first-order theory. *Computational Mechanics*, Vol.13, pp.295-314.

**Iura, M.; Atluri, S.N.** (1988): Dynamic analysis of finitely stretched and rotated 3-dimensional space-curved beams. *Computers & Structures*, Vol. 29, pp.875-889

**Iura, M.; Atluri, S.N.** (1992):Formulation of a membrane finite element with drilling degrees of freedom. *Computational Mechanics*, Vol.9, pp.417-428.

**Iura, M.; Atluri, S.N.** (2003): Advances in finite rotations in structural mechanics. *CMES:Computer Modeling in Engineering & Sciences*, Vol.4, pp.213-215.

**Kim, K.D.; Lomboy, G.R.** (2006): A co-rotational quasi-conforming 4-node resultant shell element for large deformation elasto-plastic analysis. *Computer Methods in Applied Mechanics and Engineering*, Vol.195, pp. 6502–6522.

**Kondoh, K.; Tanaka, K.; Atluri, S.N.** (1986): An explicit expression for the tangent-stiffness of a finitely deformed 3-D beam and its use in the analysis of space frames. *Computers & Structures*, Vol.24, pp.253-271.

**Kondoh, K.; Atluri, S.N.** (1987): Large-deformation, elasto-plastic analysis of frames under nonconservative loading, using explicitly derived tangent stiffnesses based on assumed stresses. *Computational Mechanics*, Vol.2, pp.1-25.

**Nguyen-Van, H.; Mai-Duy, N.; Tran-Cong, T.** (2009): An improved quadrilateral flat element with drilling degrees of freedom for shell structural analysis. *CMES:Computer Modeling in Engineering & Sciences*, Vol.49, pp.81-110.

**Oral, S.; Barut, A.** (1991): A shear-flexible facet shell element for large deflection and instability analysis. *Computer Methods in Applied Mechanics and Engineering*, Vol. 93, pp. 415-431.

**Pian, T.H.H.** (1964):Derivation of element stiffness matrices by assumed stress distribution. *Journal of AIAA*, Vol. 2, pp. 1332-1336.

**Punch, E.F.; Atluri, S.N.** (1984): Development and testing of stable, invariant, isoparametric curvilinear 2-D and 3-D hybrid-stress elements. *Computer Methods in Applied Mechanics and Engineering*, Vol.47, pp.331-356

**Reissner, E.** (1953): On a variational theorem for finite elastic deformations, *Journal of Mathematics & Physics*, Vol. 32, pp. 129-135.

**Shi, G.; Atluri, S.N.** (1988): Elasto-plastic large deformation analysis of space-frames: a plastic-hinge and stress-based explicit derivation of tangent stiffnesses.

*International Journal for Numerical Methods in Engineering*, Vol.26, pp.589-615.

**Shi, G.; Voyiadzis, G.Z.** (1991): Geometrically nonlinear analysis of plate by assumed strain element with explicit tangent stiffness matrix. *Computers & Structures*, Vol.41, pp.759-763.

**Simo, J.C.** (1993): On a stress resultant geometrically exact shell model. Part VII: Shell intersections with 5/6-DOF finite element formulations. *Computer Methods in Applied Mechanics and Engineering*, Vol.108, pp.319-339.

**Xue, W.M.; Karlovitz, L.A.; Atluri, S.N.** (1985): On the existence and stability conditions for mixed-hybrid finite-element solutions based on Reissners variational principle. *International Journal of Solids and Structures*, Vol.21, pp.97-116.

**Yang, HTY.; Saigal, S.; Masud, A.; Kapania, R.K.** (2000): A survey of recent shell finite elements. *International Journal for Numerical Methods in Engineering*, Vol.47, pp.101-127.

**Zhang, Y.X.; Cheung, Y.K.** (2003): Geometric nonlinear analysis of thin plates by a refined nonlinear non-conforming triangular plate element. *Thin-Walled Structures*, Vol.41, pp.403-418.

## Appendix

MatLab codes for generating the explicit expression of the matrix  $\mathbf{R}_\sigma$  in Eq.(53)

```
clear
%trial function of the generalized stresses
syms x y;
syms B1 B2 B3 B4 B5 B6 B7 B8 B9 B10 B11 B12 B13;
B=[B1;B2;B3;B4; B5;B6;B7; B8;B9;B10; B11;B12;B13];
str1=B1;
str2=B2;
str3=B3;
str4=B4;
str5=B5+x*B6+y*B7;
str6=B8+x*B9+y*B10;
str7=B11+x*B12+y*B13;
str=[str1;str2;str3;str4;str5;str6;str7];
%trial function of the displacements
syms u1 u2 u3 u4 u5 u6 u7 u8 u9;
syms u10 u11 u12 u13 u14 u15 u16 u17 u18;
disp=[u1;u2;u3;u4;u5;u6;u7;u8;u9;u10;u11;...
      u12;u13;u14;u15;u16;u17;u18];
```

```

%
syms x1 x2 x3 y1 y2 y3 d1 d2 d3
syms a1 a2 a3 b1 b2 b3 c1 c2 c3 A
%Calculation of the integration of the element side
pr1=SideIntegration(str,disp,1); %side 1-2
pr2=SideIntegration(str,disp,2); %side 2-3
pr3=SideIntegration(str,disp,3); %side 3-1
%Calculation of the integration over the triangular element
prb=AreaIntegration(str,disp);
%
pr=simplify(pr1+pr2+pr3+prb);
Rs=simplify(DealRs(pr)); %matrix Rs
%%
function [pr]=SideIntegration(str,disp,i)
syms B1 B2 B3 B4 B5 B6 B7 B8 B9 B10 B11 B12 B13;
syms b1 b2 b3 c1 c2 c3 A d1 d2 d3
syms x1 x2 x3 y1 y2 y3 x y s;
%
Fi1=1-s;Fi2=s;
%directions of the element boundaries
e1=c3/d1;k1=-b3/d1;
e2=c1/d2;k2=-b1/d2;
e3=c2/d3;k3=-b2/d3;
%
st5d1=diff(str(5),x);
st6d2=diff(str(6),y);
st7d2=diff(str(7),y);
std=[st5d1 st6d2 st7d2];
%
switch i
case 1 %for side'1-2'
L=d1;ca=e1;sa=k1;
x=x1+c3*s;y=y1-b3*s;
case 2 %for side'2-3'
L=d2;ca=e2;sa=k2;
x=x2+c1*s;y=y2-b1*s;
case 3 %for side'3-1'
L=d3;ca=e3;sa=k3;
x=x3+c2*s;y=y3-b2*s;
end %switch

```

```

%
H10=1-3*s^2+2*s^3; H20=(3*s^2-2*s^3);
H11=(s-2*s^2+s^3)*L; H21=(s^3-s^2)*L;
%
syms ts ts1 ts2 tn1 tn2;
j=i-1;
if i==3 j=-1; end
%
ts1= ca*disp(4+6*(i-1))+sa*disp(5+6*(i-1));
tn1=-sa*disp(4+6*(i-1))+ca*disp(5+6*(i-1));
ts2= ca*disp(10+6*j)+sa*disp(11+6*j);
tn2=-sa*disp(10+6*j)+ca*disp(11+6*j);
%
u10=Fi1*disp(1+6*(i-1))+Fi2*disp(7+6*j);
u20=Fi1*disp(2+6*(i-1))+Fi2*disp(8+6*j);
u30=H10*disp(3+6*(i-1))-H11*tn1+H20*disp(9+6*j)-H21*tn2;
%
ts=Fi1*ts1+Fi2*ts2;
wds=diff(u30,s)/L;
wd1=ca*wds-sa*ts; wd2=sa*wds+ca*ts;
%
str=eval(str);std=eval(std);
N11=str(1);N22=str(2);N12=str(3);N21=str(4);
M11=str(5);M22=str(6);M12=str(7);
M11d1=std(1);M22d2=std(2);
M12d2=std(3);
%
n1=sa;n2=-ca;
pr=int(n1*N11*u10,s,0,1)+int(n2*N22*u20,s,0,1)+int(n2*N12*u10,s,0,1)...
+int(n1*N21*u20,s,0,1)+int(n1*M11d1*u30,s,0,1)-int(n1*M11*wd1,s,0,1)...
+int(n2*M22d2*u30,s,0,1)-int(n2*M22*wd2,s,0,1)...
+2*int(n1*M12d2*u30,s,0,1)-2*int(n2*M12*wd1,s,0,1);
pr=simplify(L*pr);
%%
function [prb]=AreaIntegration(str,disp)
syms B1 B2 B3 B4 B5 B6 B7 B8 B9 B10 B11 B12 B13;
syms u1 u2 u3 u4 u5 u6 u7 u8 u9 u10;
syms u11 u12 u13 u14 u15 u16 u17 u18;
syms x1 x2 x3 y1 y2 y3;
syms L1 L2 L3 A x y;

```

```

%
N12=str(3);N21=str(4);
L3=1-L1-L2;
x=L1*x1+L2*x2+L3*x3;
y=L1*y1+L2*y2+L3*y3;
%Theta 3
t3=L1*disp(6)+L2*disp(12)+L3*disp(18);
%
pr0=N12*t3-N21*t3;
%integration over the element
ele=eval(pr0);
ele1=int(ele, L1,0,1-L2); %integrate by L1
ele2=int(ele1,L2,0,1); %integrate by L2
prb=simplify(2*A*ele2);
%%
function [Rs]=DealRs(pr)
syms b1 b2 b3 c1 c2 c3 A
syms x1 x2 x3 y1 y2 y3 d1 d2 d3
%
Rs=[d1];
for ii=1:18
    u1=0;u2=0;u3=0;u4=0;u5=0;u6=0;u7=0;u8=0;u9=0;u10=0;
    u11=0;u12=0;u13=0;u14=0;u15=0;u16=0;u17=0;u18=0;
    if ii==1 u1=1; elseif ii==2 u2=1; elseif ii==3 u3=1;
    elseif ii==4 u4=1; elseif ii==5 u5=1; elseif ii==6 u6=1;
    elseif ii==7 u7=1; elseif ii==8 u8=1; elseif ii==9 u9=1;
    elseif ii==10 u10=1; elseif ii==11 u11=1; elseif ii==12 u12=1;
    elseif ii==13 u13=1; elseif ii==14 u14=1; elseif ii==15 u15=1;
    elseif ii==16 u16=1; elseif ii==17 u17=1;
    else u18=1; end
    %
    disp('row:'); disp(ii);
    for jj=1:13
        B1=0;B2=0;B3=0;B4=0;B5=0;B6=0;B7=0;
        B8=0;B9=0;B10=0;B11=0;B12=0;B13=0;
        if jj==1 B1=1; elseif jj==2 B2=1; elseif jj==3 B3=1;
        elseif jj==4 B4=1; elseif jj==5 B5=1; elseif jj==6 B6=1;
        elseif jj==7 B7=1; elseif jj==8 B8=1; elseif jj==9 B9=1;
        elseif jj==10 B10=1; elseif jj==11 B11=1; elseif jj==12 B12=1;
        else B13=1; end
    end
end

```

```
Rs(jj,ii)=eval(pr);  
end %for jj  
end %for ii
```

where  $a_i, b_i$  and  $c_i$  are defined in Eq.(37),  $d_1, d_2$  and  $d_3$  are the length of the element boundaries,  $A$  is the area of the triangular element, and  $R_s$  is *the matrix*  $\mathbf{R}_\sigma$  in Eq.(53).